INVESTIGATION OF DEFECTS IN SILICON BY MEANS OF THE POSITRON ANNIHILATION TECHNIQUE.

By

Khaled ABDURAHMAN

A Thesis
Submitted to the Faculty of Graduate Studies
in Partial Fulfillment of the Requirements
for the Degree of

MASTER OF SCIENCE

Department of Physics
University of Manitoba
Winnipeg, Manitoba

ISBN 0-315-76956-4

INVESTIGATION OF DEFECTS IN SILICON BY MEANS OF THE POSITRON ANNIHILATION TECHNIQUE

BY

KHALED ABDURAHMAN

A Thesis submitted to the Faculty of Graduate Studies of the University of Manitoba in partial fulfillment of the requirements for the degree of

MASTER OF SCIENCE

TABLE OF CONTENTS

ABSTRACT

The positron annihilation technique is used in this study as a microscopic probe to investigate vacancy-type defects in Cz-silicon material.

In examining the distribution of defects across six inch wafers which has been grown with different pull speeds, we have observed no systematic variation in the lifetime characteristics. These observations lead us to conclude that there is no obvious relationship between the pull speed and the vacancy concentration and distribution across the wafers.

The investigations of B-doped and Sb-doped materials show that vacancies can be retained after growth at a concentration of $\sim 3 \times 10^{16}$ cm^{-3}.

Rapid Thermal Annealing (RTA) and furnace annealing are found to increase the vacancy concentration. The vacancies are then trapped by oxygen cluster complexes in lightly B-doped materials and these complexes appear to have temperature dependent configuration which can be quenched-in by rapid cooling. In heavily Sb-doped materials, Sb appears to be the dominating vacancy trap.

For the thermal donor formation kinetics study, the first set of samples investigated are B-doped p-type material codoped with carbon impurity. The results show that during the thermal donor generation at 450°C the monovacancy response decreases relative to the divacancy response after 32h of annealing time. RTA of thermal donors show a complex process which begins to take place at 725°C during which the divacancies convert into monovacancies. No correlation was evident between thermal donor concentration and vacancy response.

The second set of samples investigated are B-doped without any carbon codoping. The results reveal a different effect from the C-doped samples.

ACKNOWLEDGEMENTS

The work presented in this report is carried out in partial fulfillment of the requirements for obtaining the MASTER OF SCIENCE (MSc.) degree under the supervision of professor S. Dannefaer.

I wish to express my sincere thanks to Prof. S. Dannefaer for the valuable advice and for his patient guidance and constant encouragement throughout this research.

Sincere thanks are also due to Dr. T. Bretagnon for his valuable advice, assistance and for many fruitful discussions.

I also wish to extend my thanks to Dr. S. Hahn for supplying the samples used in this thesis.

Thanks are also due to Dr. J. Vail and Dr. D. Thompson, both for their valuable advice and their willingness to examine this work.

I am especially most grateful to my parents, my wife, and my friends for their sincere encouragement and continous support.

I wish to express appreciation to the Secretary of Scientific Research in Libya for the financial support given to me during the course of my studies.

Finally I express my deep debt and gratitude to Allah for making this work a success.

CHAPTER ONE

INTRODUCTION TO POSITRON ANNIHILATION AND DEFECTS

CHAPTER ONE

1.1. INTRODUCTION

The discovery of the positron, or antielectron, was an important consequence of the theoretical and experimental development of quantum mechanics in physics.

The story began in 1926 when Gordon and Klein formulated a relativistic quantum mechanical theory, which gave negative energy solutions for the electron (1). Four years later Dirac published "A Theory of Electrons and Protons" where he postulated his famous "hole" theory, in which the positron was viewed as a missing electron (a "hole") in the "sea" of electrons all with negative energy. Dirac stated in this theory that an electron (with positive energy) could jump into the "hole", and energy will be released by emission of γ-quanta. Dirac's equation had two solutions for the total energy of the electron, $E=\pm(p^2c^2+m_o^2c^4)^{1/2}$, where p is the momentum of the electron, c is the velocity of light, and m_o is the rest mass of the electron. The energy would reach values between $m_oc^2 \rightarrow \infty$ and $-m_oc^2 \rightarrow -\infty$. The continuum of states from $-m_oc^2 \rightarrow -\infty$ was occupied by electrons with negative energies. When a γ-ray with an energy larger than $2m_oc^2$ interacts with one of the electrons with negative energy, the electron would be lifted into a positive state, leaving a "hole" which would behave as a positively charged particle (2). The annihilation process takes place by the falling-down of the electron with positive energy into the "hole", and γ-quanta with a total energy of $E=2m_oc^2+E_+ +E_-$ (where m_oc^2 is the rest mass of electron and positron, and E_+, E_- is the kinetic energy of the positron and electron respectively) would be emitted (see figure 1.1 Ref. 149).

In 1933 Anderson showed experimentally the existence of a positively charged particle with a mass similar to the mass of an electron by using the Wilson cloud chamber (3). In the presence of a strong magnetic field, the tracks on a photographic plate were observed to be caused by a

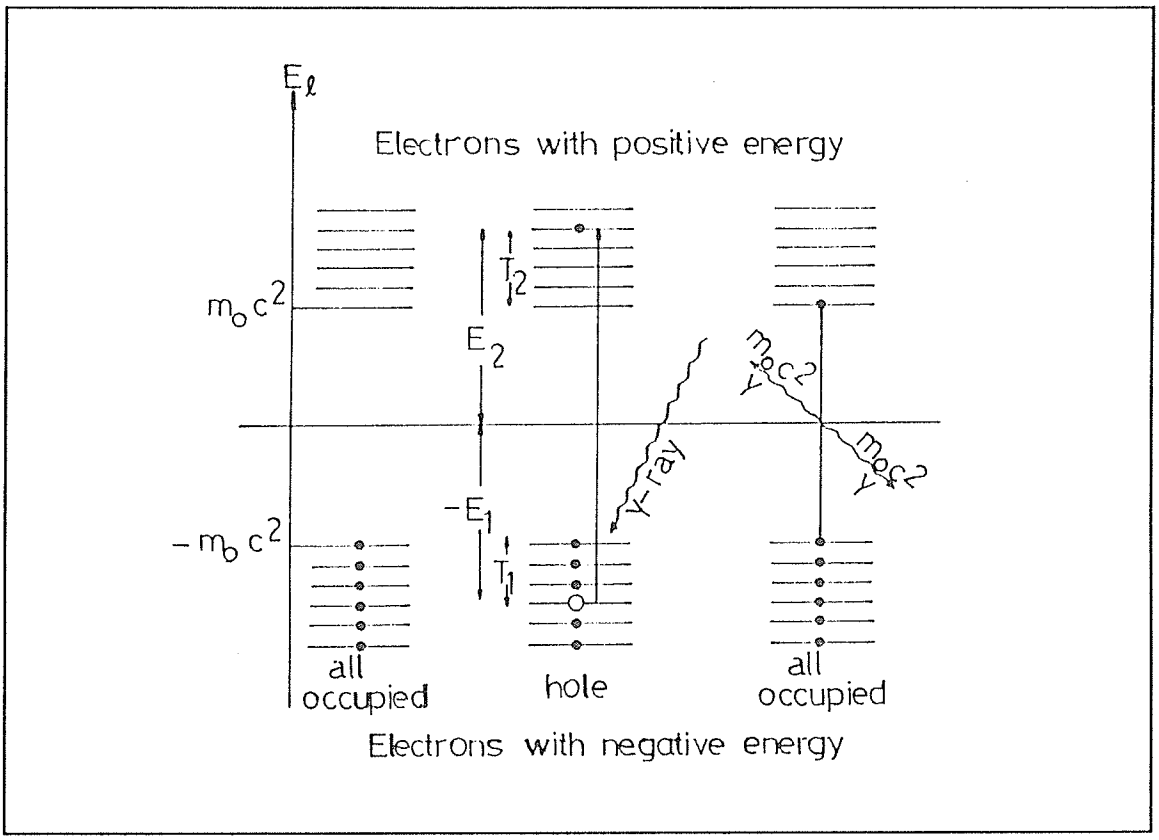

Figure 1.1 : A schematic representation of "Hole-Theory".

positively charged particle which had a mass closer to that of the electron than that of the proton. Blackett and Occhialini (4) gave further experimental evidence of the existence of the positron in a paper published in 1933 which confirmed the observations of Anderson. One year later, it was shown by Thibaud (5) that the positron could annihilate with an electron by emission of two γ-quanta, each with an energy of 0.511 Mev. Klemperer also demonstrated that the quanta were emitted in coincidence and in opposite directions (6). For further readings on the discovery of the positrons, see reference (7).

The applications of the positron annihilation techniques (PAT) for the study of materials began in 1942 when De Benedetti *et al* (8) investigated the lifetime of positrons in different metals. From that time on the positron annihilation technique became a very useful probe in the field of defect studies of materials. The technique proved to be very sensitive to different vacancy type

defects such as vacancies, vacancy clusters, voids, and possibly dislocations. The non destructive feature of this method gives an important advantage in extracting information about the nature and the concentration of defects which may be revealed in the characteristics of the positron annihilation. There are usually three methods of positron annihilation used in order to extract information about the annihilation quanta (see figure 1.2 Ref. 149); Doppler broading measurements, the angular correlation measurements (these two methods give information about electron momenta), and the positron lifetime measurements. The work presented in this thesis deals only with the use of the positron lifetime measurements which gives information about the electron density. The method will be explained in more detail in the following chapters.

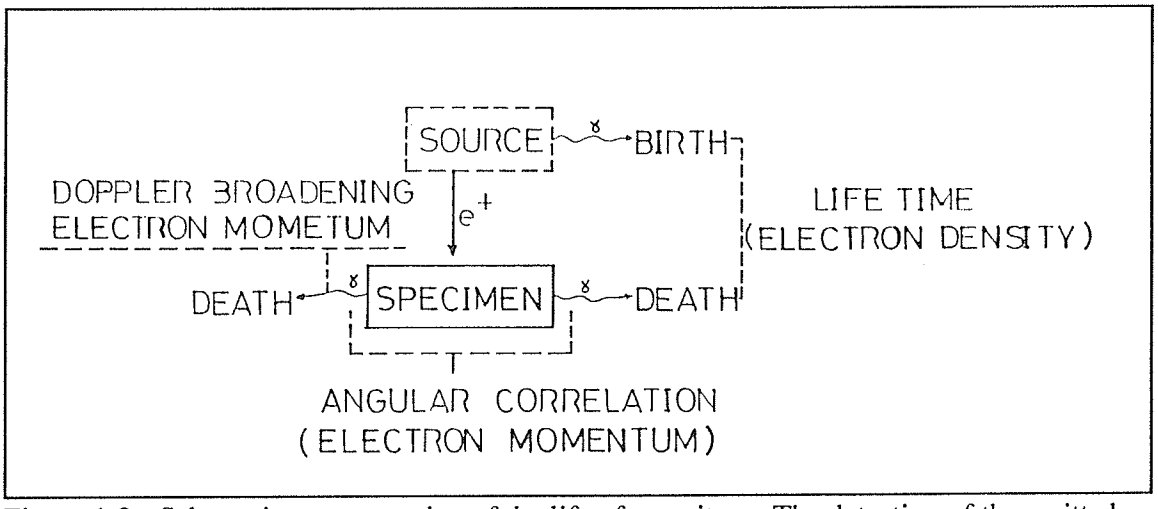

Figure 1.2 : Schematic representation of the life of a positron. The detection of the emitted γ-quanta is the base of positron annihilation technique.

What is a defect? A great deal of work had been carried out by scientists in this field in order to find out the nature of a defect. The crystalline defect generally speaking means any region where the microscopic arrangement of ions differs drastically from that of a perfect crystal (9). The defects are classified into three categories ; Point defects, line defects, and surface defects, according to whether the imperfect region is bounded on the atomic scale in one, two, or three dimensions. There is a wide variety of defects but we will mainly be investigating in this work

the point defects, more specifically vacancies and vacancy clusters. Vacancies and interstitials are point defects consisting of the absence of ions or presence of extra ions. Their presence is a normal thermal equilibrium phenomenon, so they can be an intrinsic feature of real crystals. Such defects are responsible for the observed electrical conductivity of ionic crystals, and also can alter their optical properties. Another type of defects we may briefly come across is dislocations. The dislocation is the line of demarcation between two regions of a crystal, one of which has slipped relative to the other (10). These defects can be produced when a crystal is irradiated by sufficiently energetic particles (radiation damage) or by deformation. Dislocations are responsible in explaining the observed strength (or rather the lack of shear strength) of real crystals. The illustrations of different kinds of defects are shown in chapter four.

Metals are characterized by high electrical conductivity, because a large number of electrons in a metal is free to move. These free electrons are called conduction electrons. The outer electrons of the atom become the conduction electrons of the metal (11). Metallic conductivity is typically between 10^4 and 10^6 $(\Omega cm)^{-1}$ while typical insulators have conductivities of less than 10^{-10} $(\Omega cm)^{-1}$. Some solids with conductivities between 10^{-10} and 10^4 $(\Omega cm)^{-1}$ are classified as *semiconductors*. These are covalently bonded. Without going into a lengthy discussion on this subject, since it is beyond the scope of this work, the important feature is that semiconductors have an *energy gap* between the valence and the conduction energy bands while semi-metals and metals have no such gap. The difference between semiconductors and insulators is a matter of the numerical value of the energy gap. As the temperature approaches absolute zero, pure semiconductors become insulators. Likewise the semiconductors become nearly metallic when heavily doped. Typical elemental semiconductors are silicon, diamond and germanium all belonging to the fourth group of the periodic table. In the third group, the lightest element boron is also considered semiconductor. The lightest element of the fifth group is antimony, which may

be classified as semiconductor (12). The behaviour of semiconductors is not restricted only to solids, but there are compound, liquid, and some aromatic hydrocarbon semiconductors. Further explanation will be given in the following chapters regarding the physics of semiconductors.

The study of defects in semiconductors and metals has mainly three goals ; (1) the identification of the defects, (2) the understanding of how the defects are introduced (and removed), and (3) the understanding of the changes in the physical properties caused by those defects. There are many techniques by which defects are introduced into semiconductors and metals, eg., quenching for high temperatures, plastic deformation, irradiation by neutrons, by heavy charged particles or by electrons, thermal annealing and other techniques as well (13). Quite generally, a semiconductor is *intrinsic* if its electronic properties are dominated by electrons thermally excited from the valence to the conduction band, and *extrinsic* if its electronic properties are dominated by electrons contributed to the conduction band by impurities (or captured from the valence band by impurities). Impurities that contribute to the carrier density of a semiconductor are called *donors* if they supply additional electrons to the conduction band, and *acceptors* if they supply additional holes to i.e., capture electrons from the valence band (14).

In an n-type semiconductor the impurity or donor atoms have one more valence electron than the atoms composing the crystal lattice. These donor atoms readily donate their extra valence electron to the conduction band, thus producing mobile electrons in the conduction band to carry current and positively charged donor atoms or ions locked in the lattice. In a p-type semiconductor the impurity or acceptor atoms have one less valence electron than the atoms composing the lattice. These acceptor atoms readily attract electrons from the valence band, thus producing mobile positive holes in the valence band to carry current and negatively charged acceptor atoms or ions locked in the lattice (15). The charge state of a defect corresponds to the number of the carriers which remain localized on the site of the defect. The concentration of a

defect in a given charge state is determined by the position of the Fermi level as compared to the position of the localized electronic state associated with the defect. Thus, the charge state will depend on the temperature, the doping impurity concentration and the concentrations of other deep levels (16). Defects in semiconductors can have a positive charge which will make them undetectable for the positrons.

CHAPTER TWO

POSITRON PHYSICS

CHAPTER TWO

2.1 Annihilation of positrons

When a positron from the radioactive source is injected into a sample, the kinetic energy is usually several hundred keV. This energy is rapidly lost by collisions with the atoms of the medium, (the slow-down process) which normally takes 10^{-11} to 10^{-12} sec in solids. Only a very small portion of positrons annihilate during this process (17). The mean implantation range is typically 100μm. The thermalized positrons can annihilate through several processes. They may annihilate from a free state or from some bound state within a molecule or a defect, or they may annihilate from a state where it is bound to one electron only (this bound state is the so-called positronium atom). The lifetime of positrons is characteristic of each material and varies from

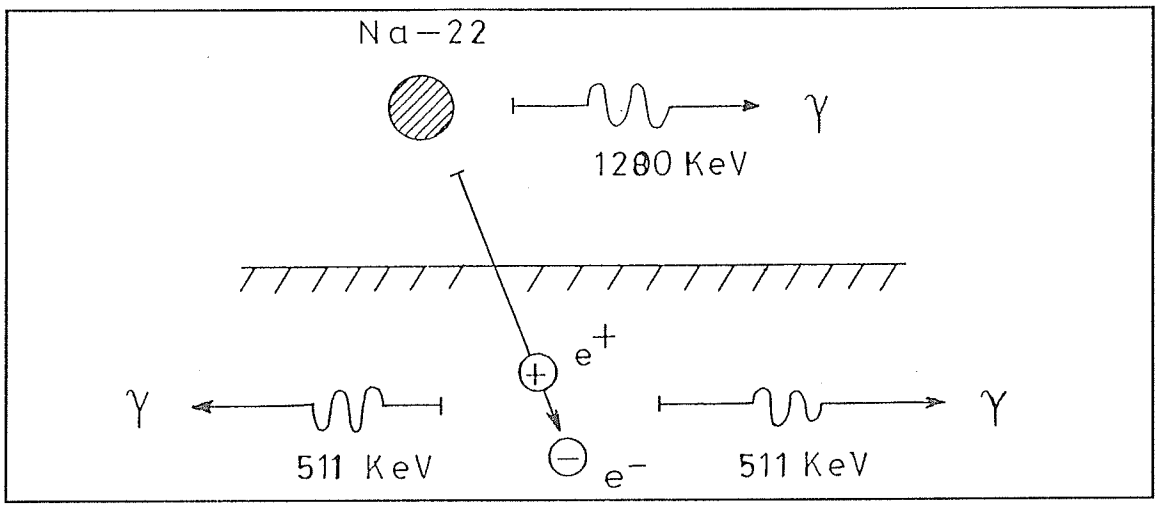

Figure 2.1 : Positron annihilation lifetime experiment.

100 to 500 ps. Figure 2.1 (Ref. 18) shows schematically the positron annihilation lifetime experiment. The positrons from the most commonly used radioactive isotope ^{22}Na annihilate in the sample material. The nucleus emits a 1.28 MeV photon within a few picoseconds after the

positron emission which serves as a birth signal. The time delay between the birth and the subsequently emitted annihilation gammas is the lifetime measurement of the positron. The momentum of the annihilating electron-positron pair can be detected as a small angle deviation from collinearity between the two 511 keV photons. The motion of the pair also causes a Doppler shift of the annihilation radiation and can be detected by an accurate energy measurements of one of the photons (18).

The positron-electron annihilation is a quantum phenomena where the particle masses are converted into electromagnetic energy. There are several ways in which the annihilation of a positron with an electron will occur. One-gamma annihilation is possible only in the presence of other bodies, which absorb the recoil momentum. This process is very rare, and it is mainly interesting from a theoretical point of view. The main process is the two-gamma annihilation which requires that the photons are emitted in opposite directions in the centre of the mass system in order to conserve momentum, each of the gamma rays carrying half of the energy of the process. The three-gamma annihilation is important only in a spin-correlated state like ortho-positronium, where the selection rules forbid the two-gamma annihilation process.

From the non relativistic limit of the 2 γ-annihilation cross section derived by Dirac one obtains the annihilation probability per unit time or the annihilation rate $\lambda = \pi r_o^2 c n_e$ which is independent of the positron velocity. Here r_o is the classical electron radius, c the velocity of light and n_e is the electron density at the site of the positron. The electron density of the medium can, however, not be obtained by determining the annihilation rate λ, because the opposite charges of the electron and the positron creates a strong enhancement of the local electron density n_e from the equilibrium value. Calculation of these positron-electron correlations is a complicated many-body problem which is well understood only in the case of the electron gas (19). The enhancement is typically in the order of 4, but depends on the electron density.

2.2 Positron Thermalization

It has long been shown that when a fast positron from a radioactive source penetrates a solid, it interacts with electrons and nuclei and so losses gradually its kinetic energy until it becomes thermalized. Elastic collisions with electrons result in ionization or electronic excitations depending on the energy transferred to the electrons. In inelastic collisions with nuclei, a positron can lose energy by emitting radiation, by creating phonons or even by atomic displacements. Thermalization justifies the assumption that the momenta of positrons are small compared to the momenta of the electrons with which they annihilate. In metals, electron excitation dominates the inelastic-scattering process. The stopping power, S=-dE/dx, ie. the energy loss per unit distance traversed of a medium for swift particles is usually calculated in terms of a "continuous slowing-down approximation", according to which energy losses occur almost continuously in small portions through collisions with electrons in the medium.

The stopping power, which is practically constant and equal to 1MeV/gcm between 0. 1 and 10 MeV, increases by one order of magnitude when E decreases from 0. 1 MeV to 0. 1 keV according to the Bethe expression :

$$-\frac{dE}{dx}=\frac{2\pi e^4 NZ}{E}\ln(\frac{1.16E}{I})$$

where I is the mean excitation energy and N the density of atoms with atomic number Z. The mean energy loss per path length after reaching a maximum value around $E\approx 20eV$ decreases very rapidly. In metal that decrease results from the fact that core ionization and plasmon excitation disappear. Moreover, below 10 eV the electron-hole excitation becomes less efficient since its energy loss rate decreases as E^2. In metals, electron hole scattering remains allowed until thermal energies. In insulators electron hole excitation is limited to positron energies larger

than the energy gap. To achieve complete positron thermalization, phonon creation becomes the predominant process. In any case, the mean energy loss rate of epithermal positrons is a rapidly decreasing function of the positron energy. The total thermalization time $\tau_{th}=10^{-11}$s is nevertheless short compared to the lifetime of positron in matter $\tau \geq 10^{-10}$s (20).

The depth distribution of the thermalized positrons in the sample is well described by:

$$dp(x)=\alpha \exp(-\alpha x)dx \tag{1}$$

where x is the distance from the surface of the sample and α is given by:

$$\alpha=17\rho/E_{max}^{1.43} \qquad [cm^{-1}] \tag{2}$$

E_{max} is the end point energy of the positrons (0. 54 MeV) and ρ is the density of the samples in g/cm^3. For silicon α equals $96cm^{-1}$, which means that essentially all positrons annihilate within a depth of 0.2mm (the average penetration depth is $1/\alpha=0.1$ mm for silicon). The ^{22}Na positron source is therefore only suitable for bulk studies and can not practically be used for investigations of thin films ($< 10\mu$m) or surfaces. For such studies slow positron beams are used with kinetic energy tunable from a few eV to several keV (21).

2.3 Positron Lifetimes

The rate by which the annihilation take place is :

$$\lambda=\pi r_o^2 c \int |\psi_+(r)|^2 n_e(r) d^3r \tag{3}$$

where r_o is the classical radius of electron, c the speed of light, $\psi_+(r)$ positron wave function, and $n_e(r)$ the electron density. It must be stressed that $n_e(r)$ is the electron density determined

self consistently with the presence of the positron. This is important since the positron locally enhances the electron density easily by a factor of two. The calculations of the positron wave function and annihilation rates in metals and semiconductors (22,23) show that the positron wave function is peaked in the interstitial regions between the atoms. This result is expected when one considers that the potential which excludes the negatively charged electrons from the interstitial region will have the opposite effect on the positively charged positrons.

2.4 Trapping by Defects

Positrons can be trapped in a material that contains defects. Trapping occurs typically for vacancy-type defects because the positron energy is reduced relative to the untrapped state due to a reduced overlap between the positively charge ion core and the positively charged positron. The binding energy is the order 0-1 eV which vary considerably with the morphology of the defect. There are a few experimental indications for trapping by interstitial related defects, but theoretical calculations on specific systems are lacking as yet. Positron traps can be divided into two categories: Deep traps where the binding energy is much larger than thermal energy at 300K (1/40eV) and shallow traps where the energies are comparable. A distinct aspect encountered in semiconductors (and not in metal) is that only neutral or negatively charged defects are responsible for trapping positrons.

2.5 Model for Trapping

There are two fundamentally different models for describing the trapping mechanism of positrons: the statistical model and the trapping model.

2.5.1 The statistical model

In this model one assumes that an ensemble of positrons during or at the end of the thermalization process have become trapped at various defects or reside in the bulk. However, the work of this thesis was carried out using the trapping model only, to be described below.

2.5.2 The trapping model

In contrast to the statistical model, the trapping model (24-26) uses the assumption that all positrons are in only one state at the time of thermalization (t=0). This state is a delocalized Bloch state (see Fig. 2. 2). When defects are present in the sample material under investigation, positrons are assumed to be transferred from the Bloch state (commonly referred to as the bulk state) to a defect with trapping rate κ_i proportional to defect concentration C_i.

$$K_i = \mu_i C_i \qquad (4)$$

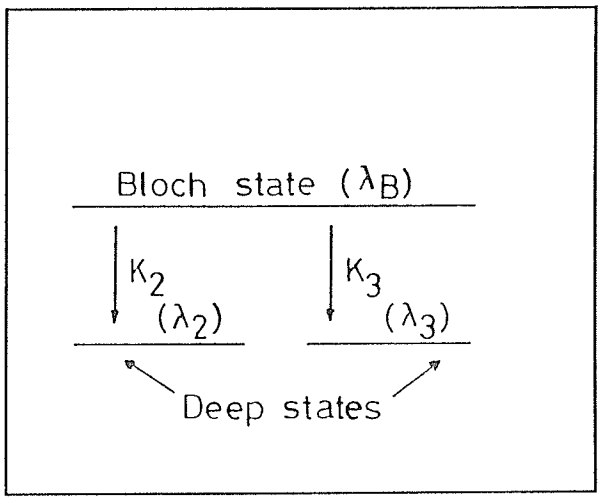

Figure 2.2 : Trapping from Bloch state into two different traps with trapping rates κ_2 and κ_3.

where C_i is the number of defects of type "i" per unit volume and μ_i is called the specific trapping rate.

The occupation probability for positrons in the bulk state n_B and in the defect state n_i can be expressed by the following differential equations:

$$\frac{dn_B}{dt} = -\lambda_B n_B - n_B \sum_i^N \kappa_i \qquad i=1,2,..,N \qquad (5)$$

$$\frac{dn_i}{dt} = -\lambda_i n_i + \kappa_i n_B \qquad (6)$$

where λ_B is the annihilation rate in the bulk state and $\Sigma\kappa_i$ is the total trapping rate due to the

different type of defects.

The first term in equation (5) describes that positrons disappear from the bulk state by annihilation whereas the second term describes that positrons disappear from the bulk state by the transfer to an other state. Also, equation (5) assumes that detrapping does not take place because the traps are deep.

The total occupation probability can be obtained by solving the coupled differential equations using the boundary conditions at $t=0$, $n_B=1$ and $n_i=0$.

Thus;

$$n(t)=[1-\sum_i \frac{\kappa_i}{\lambda_B-\lambda_i+\sum_n \kappa_n})\exp[-(\lambda_B+\sum_n \kappa_n)t]+\sum_i \frac{\kappa_i}{\lambda_B-\lambda_i+\sum_n \kappa_n}\exp(-\lambda_i t) \qquad (7)$$

Where the terms in front of the exponentials are called the intensities of the lifetime components and have the sum one. Since the annihilation of positrons are detected, a lifetime spectrum will then have the theoretical form

$$S(t)=\frac{-dn(t)}{dt} \qquad (8)$$

A very important consequence of the trapping model is that the bulk annihilation rate, although not directly observed in a given spectrum when trapping occurs, can be calculated according to:

$$\lambda_B=\sum_1^N I_i\lambda_i \qquad (9)$$

where $\lambda_i=1/\tau_i$, and τ_i is the i'th lifetime component.

In the case of only one defect type the trapping rate can be found from:

$$\kappa = \frac{I_2}{1-I_2}\left(\frac{1}{\tau_B} - \frac{1}{\tau_2}\right) \qquad (10)$$

The three parameters τ_B, τ_2, and I_2 are determined from the least square fitting of the experimentally determined lifetime spectra.

The validity of the trapping model can be checked by using the experimental data in Eq. (9) because constant values of λ_B should be obtained regardless of the defect situation.

2.6 Applicability of the Two Models

The experimental lifetime spectra are analyzed using exponentially decaying terms according to:

$$S_{exp}(t) = \sum_{i}^{N} \lambda_i I_i \exp(-\lambda_i t) \qquad i = 1,2,..,N \qquad (11)$$

in accordance with Eq.(8). Here N is the number of components (usually not known a priori) that would be chosen in order to analyze the spectra. By assuming different values the choice for N is established initially by the goodness-of fit (χ^2) which must be within 1.00 ± 0.06. If, for example, N=2 satisfies this criterion, it is sometimes also possible to analyze the spectrum with N=3 with equally good value. Strictly speaking one can therefore only establish the lower limit for the number of components in a given spectrum and it is this which constitutes the major problem in the analysis of lifetime spectra, since the number of components, their lifetime and intensity value, are used for the subsequent physical interpretation of the data. In practical applications it turns out that if two lifetime component differ by only $\approx$50ps an unconstrained fit can only with difficulties separate such two components so that only some weighted average value is produced by the fitting procedure. This type of problem can often be resolved in the context of a series of measurements, but is nevertheless the primary source for uncertainties in the physical interpretation. Recent systematic studies (27) have shown that the ability for

resolving individual components is strongly dependent on the quality of the lifetime spectra, i. e. spectra with large amounts of counts ($>5x10^6$), good time resolution (<270 ps) and weak radioactive source strength ($< 5\mu$Ci) significantly alleviates these problems.

2.7 Sensitivity to Defect Concentrations

Defects that are present in the sample material can be detected and measured if their concentrations level is generally above 0. 1 ppm. For instance, in metals the specific capture rate is in the order of10^{15} to $10^{16}s^{-1}$ per unit fractional defect concentration. In semiconductors the capture rate for neutral defects is somewhat smaller ($\sim 5x10^{14}$ s^{-1}), but for negatively charged defects the rate increases significantly especially at low temperature according to a $(T/300)^{-2}$ dependency relation (28). For example at 30K the capture rate for negatively charged defects is thus $\sim$100 times higher than at room temperature.

CHAPTER THREE

EXPERIMENTAL APPARATUS

CHAPTER THREE

3. 1. Description of the lifetime equipment

The lifetime measuring system consists of advanced electronics in the so-called fast-fast time coincidence system. A typical block diagram is shown in Figure 3. 1 where we can see that the

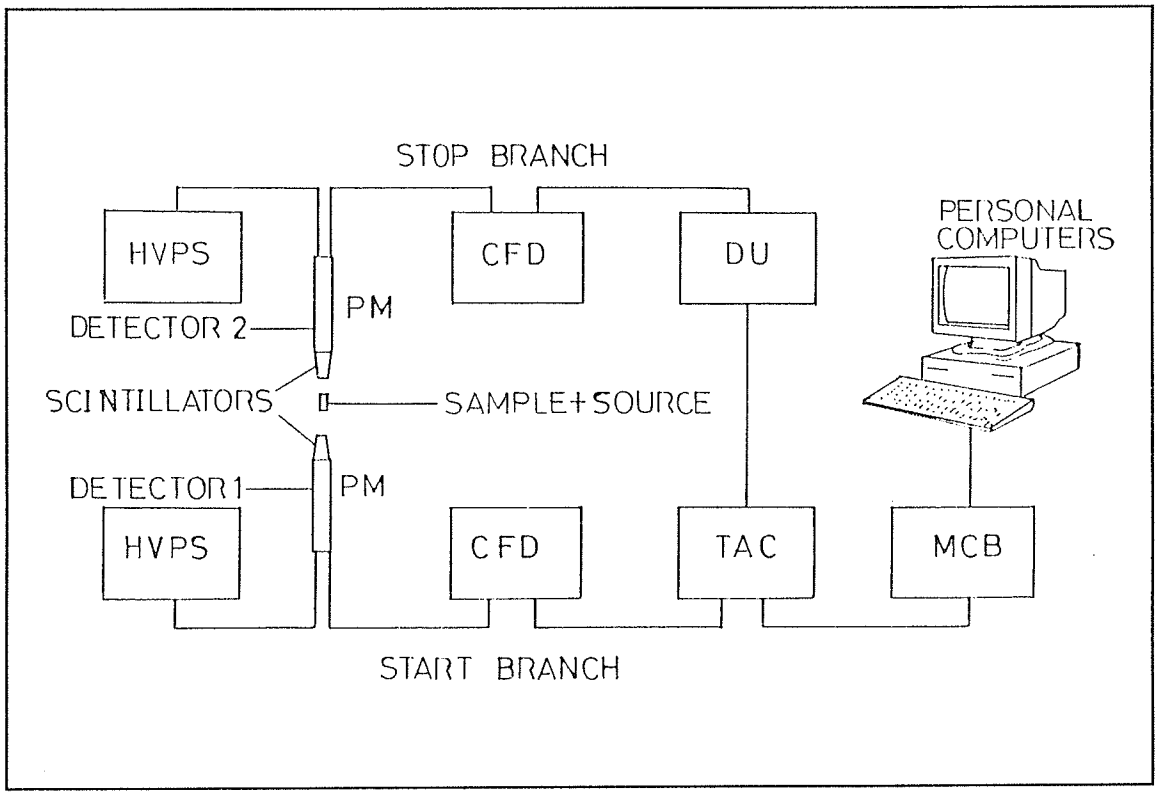

Figure 3.1 : Block diagram of a lifetime equipment.
(HVPS: High Voltage Power Supply;PM Phoromultipliers TAC: Time to Amplitude Converter; MCB: Multichannel Board; CFD: Constant Fraction Discriminator; DU: Delay Unit).

lifetime measuring system is divided into two branches; The start branch and the stop branch which will be connected to the detector #1. The anode signal from detector #1 is fed into a discriminator circuit (Constant Fraction Discriminator CFD) which gives an output pulse when the anode signal falls within a preset pulse height range. The output from the CFD is then fed

into a time-to-amplitude converter (TAC). The stop branch is quite similar to the start branch except that the output from the CFD is connected to a precision delay unit. The delayed signal is then connected to the TAC for conversion. The output of the TAC is a pulse whose amplitude is proportional to the time difference between the two input signals which will be processed and stored by the multi-channel-analyzer (MCA). The collected data from the MCA will be then fed into a personal computer for analysis.

In our laboratory there are three different lifetime spectrometers. The stop branches utilize Ortec 583 constant fraction discriminators (CFD) while the start branches use a single Ortec 934 quad constant fraction discriminator, since this discriminator only has the possibility for setting a lower threshold level.

3. 2. Source preparation

The most widely used positron source for this kind of measurements is the source nucleus ^{22}Na isotope. The decay scheme of ^{22}Na is shown in Figure 3. 2, (Ref. 150). The preparation of the positron source is done by evaporating a few micro curies of aqueous solution $^{22}NaCl$ onto a thin aluminum foil (around 1μm thick) wrapped as a square envelope of approximately 1x1 cm^2 around the source. For the purpose of our experiments, a number of sources were made ranging in strength between 8-10 μCi. In all experiments the source was placed between two identical samples (the sandwich technique).

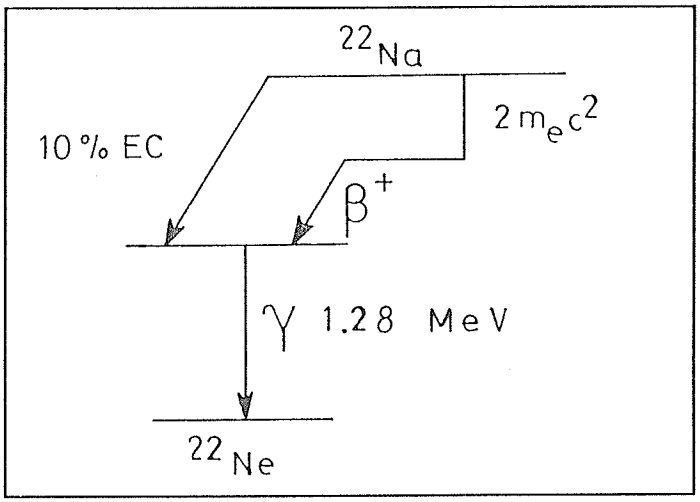

Figure 3.2 : Decay scheme for ^{22}Na.

3. 3. An overview of operation and performance

The lifetime measurement is the determination of the time elapsed between the emission of a positron from the ^{22}Na source and its subsequent annihilation. The "birth" gamma photon has an energy of 1. 28 MeV emitted simultaneously with the positron from the source nucleus (^{22}Na isotope) and the two "death" (annihilation) quanta have each an energy of 0. 511 MeV.

3. 3. 1. Photomultiplier (PM) and Scintillator

The detection of the gamma quanta is accomplished by a plastic scintillator mounted to a photomultiplier tube. The new Hamamatsu tubes (H2341) have been shown to be of superior quality (29). For most of the tubes the high voltage was not critical. For one tube, however (start in system II) the high voltage had to be quite low in order to obtain a resolution function free of a tail. This tube has an exceptionally high amplification. In order to obtain a good time resolution it is necessary to use scintillators which have a fast-decaying light pulse. One such scintillator is called Pilot U manufactured by Nuclear Enterprises. The pilot U scintillators were machined in different sizes in order to obtain different efficiencies and were polished to a mirror-like finish. No paint was applied to the surfaces in order to obtain spectral reflection of light. This results in a sharper time distribution of the light intensity than if a diffusing coating is applied (30). The particulars of the 3 spectrometers are listed in Table I.

System I was made purposely for a narrow resolution function while maintaining a count-rate suitable for obtaining $> 5x10^6$ counts during 16 hours of spectrum accumulation. System II, and in particular System III employ larger scintillators and are designed primarily for low/high temperature work which requires larger (18 mm) detector separation.

A surprisingly small degradation in the width of the resolution function with scintillator size is found for System II and III which indicates that the time spread arising from the scintillator is kept at a minimum and that the PM tubes perform well even when using the full size of the

SYSTEM	Branch	High Voltage	Scintillator [a]	Count rate / [b] (sec. x Ci) 4 mm	18mm	FWHM/ [c] Internsity (ps/ %)
I	stop	2300	d h d(ϕ)=40 mm h=10 mm	20.5	4.0	162/90, 205/10
	Start	2300	d(ϕ) +36 mm h=36 mm a			
II	stop	2200	d(ϕ)=40 mm h=10 mm	37.6	9.2	180/70, 260/30
	Start	1650	d(ϕ)=45 mm h=36 mm			
III	stop	2300	d(ϕ)=36 mm h=36 mm	71.6	19.2	173/70, 257/30
	Start	1900	d(ϕ)=44 mm h=50 mm			

a) All angles, are 10 degrees (shown exaggerated in the drawings)
b For collinear setup with detector distances of 4 or 18 mm
c) Assuming a 2-gaussion approximation to the resolution function

Table I : Particulars of the 3 lifetime spectrometers used.

cathode area. In our opinion one may just as well only employ the larger scintillator since this reduces significantly the accumulation time. For all 3 spectrometers the resolution functions could be described using mainly one gaussian. The second gaussian was displaced typically 30 ps to the left of the main gaussian. One of the spectrometers has now been operating continuously for 2 years and has proven very stable.

These investigations have shown that the Hamamatsu tubes perform rather well with only 1 tube out of 6 being of somewhat inferior quality (the high-gain one in System II). High count rates are achievable ≈ 70 per (sec x μCi) using large Pilot U scintillator rivalling the performance of BaF_2 based systems.

3. 3. 2. Constant Fraction Discriminator (CFD)

Each anode signal (one from each detector) is fed into a CFD which gives an output pulse when the signal exceeds a preset level. The fast detector provides the best time resolution because of its short decay time. However, this results in a very poor energy resolution of the scintillator crystals (see Figure 3.4), so that different pulse heights result. This will result in a jitter in the time for the pulse crossover of the discriminator level to take place at different times (see Figure 3. 3a Ref. 150), leading to different TAC outputs. The constant fraction discriminator is used to reduce this problem. It splits the pulses into two signals, inverting one, delaying it behind the other attenuated signal, adding them together, and detecting when the added pulses cross the base line as shown in Figure 3. 3b, (Ref. 150). The amplitude of the negative part is a constant fraction of the positive part, and the crossover point between the negative and the positive parts can be defined by the so-called walk-adjustment.

After amplification, the signal is fed into a single channel analyzer (it is built into the CFD unit) which selects a small part of the amplitude range and as output gives a standard pulse if the input signal was within the permitted window.

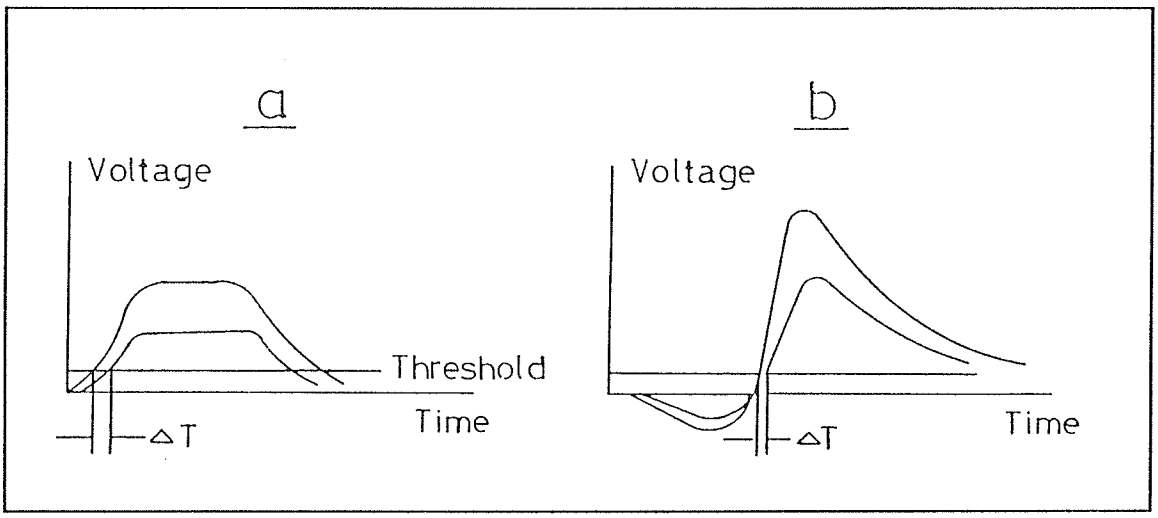

Figure 3.3 : Uncertainty in time determination due to different pulse heights by (a) leading edge system and (b) constant fraction system.

Optimal timing performance is achieved by the careful selection of the constant-fraction shaping delay cable and proper setting of the walk adjustment. Energy selection is achieved by the proper setting of the lower-level and the upper-level controls in the CFD. The proper setting values are extracted from the gamma spectrum (see Figure 3. 4), thus defining the start branch as the one which accepts only pulse amplitudes which arise from the 1.28 MeV "birth" quanta. The sharply peaked structure in Figure 3.4 arises from 0.511 MeV γ-quanta. By setting the energy levels in the other branch this branch becomes designated to detect only "death" γ-quanta. Only those detected events that satisfy these energy requirements, as well as being separated in by less than 50ns will be processed by the MCA.

3. 3. 3 Time to Amplitude Converter TAC and Multichannel Analyzer MCA

The outputs from the two CFD's are fed into the TAC unit where the time difference between the two input signals is converted to a proportional pulse height (0-10V). The output of the TAC is transferred to the MCA which consists essentially of a gate circuit, an analog to digital converter and an information storage unit. The channel number (1-2048) in the MCA is proportional to the time difference between the two γ-quanta recorded by the detectors. The

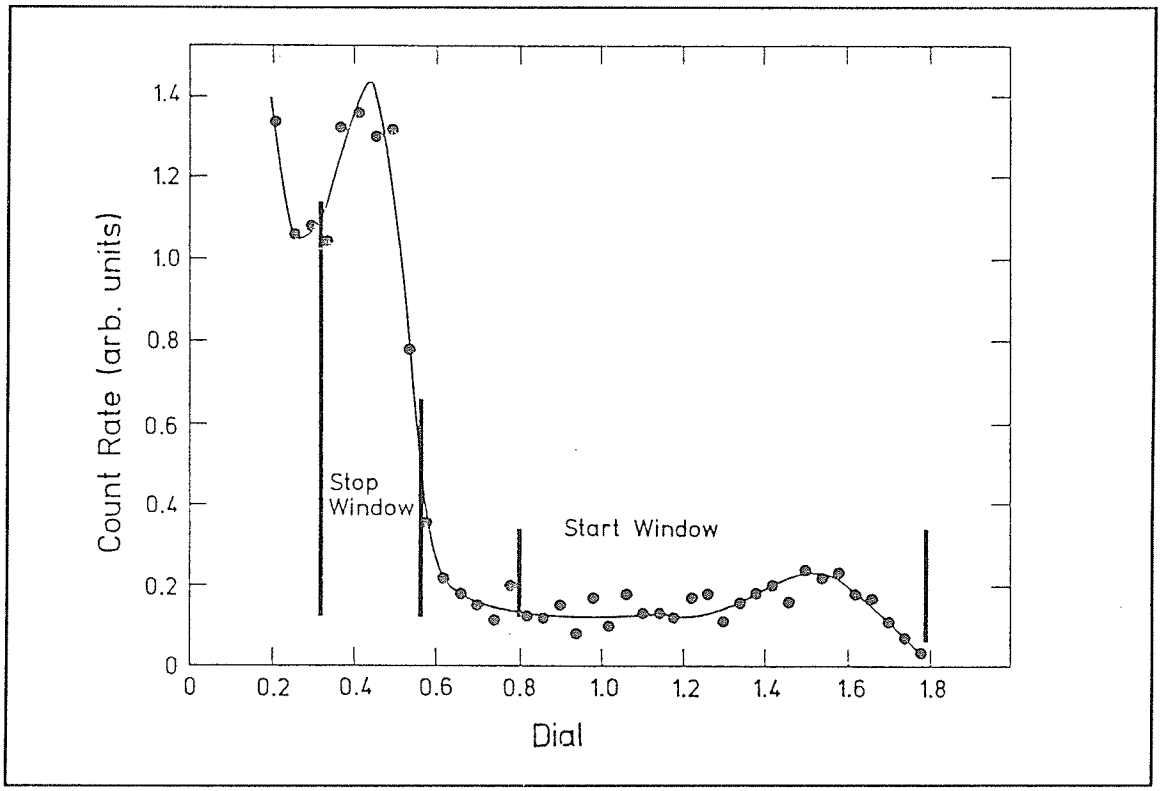

Figure 3.4 : Gamma spectrum.

number stored in each channel is the number of events recorded with a certain time difference ie. the number of positrons that lived a certain time.

3. 4. Positron Lifetime Spectrum

The positron lifetime measurement is the determination of the time elapsed between the emission of the positron (birth signal 1.28MeV) from ^{22}Na source when it undergoes a β-decay and it annihilates as signalled by the annihilation quanta (death signal 0.511MeV). This time is typically between zero and five nano seconds (1ns = 10^{-9} s), and by recording the annihilation for many individual positrons, one obtains the so-called lifetime spectrum, an example of which is shown in Figure 3.5. In addition to the lifetime spectrum, a certain random background will be recorded due to the fact that the annihilation of the two different positrons can be detected as a coincidental event.

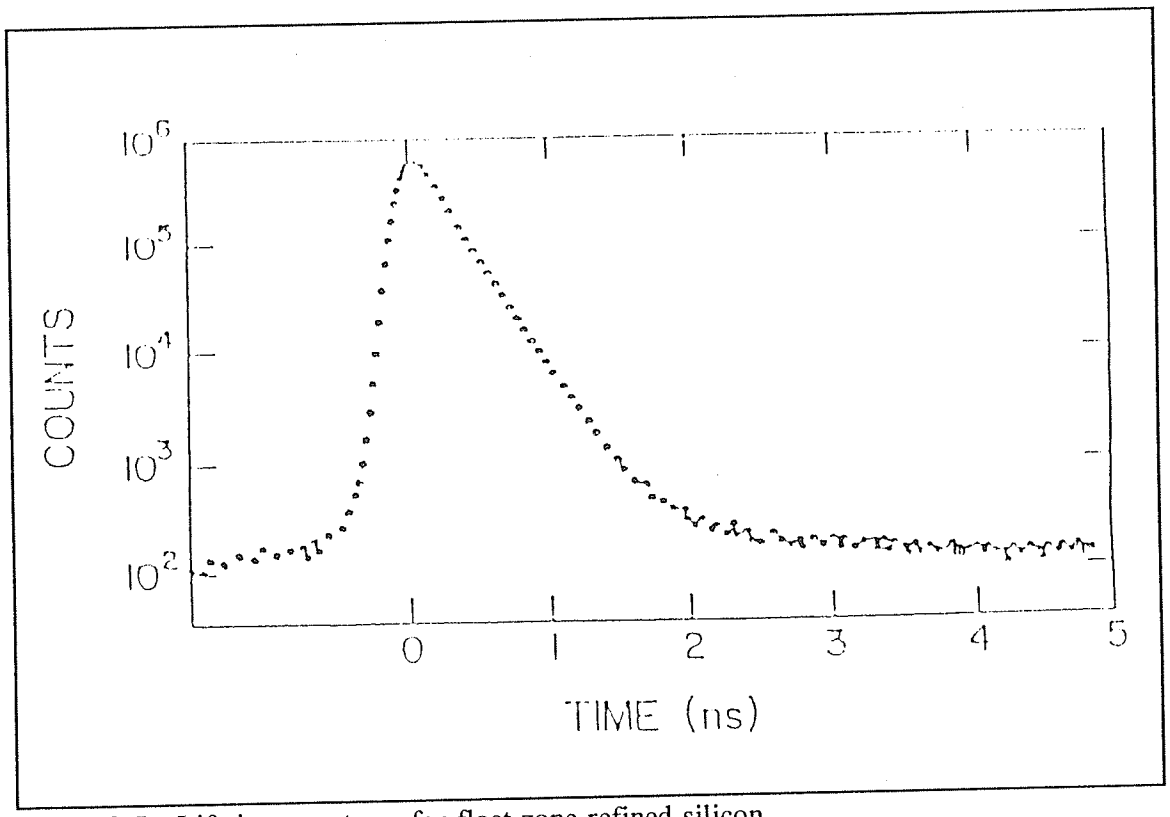

Figure 3.5 : Lifetime spectrum for float-zone refined silicon.

3. 4. 1. Time resolution

The time resolution of a system is normally defined as the full width at half maximum (FWHM) of the so called prompt curve which is obtained from a ^{60}Co source emitting two γ-quanta simultaneously, and would with infinite resolution power be delta-like, but as the resolution power is finite for an actual equipment one measures a curve with a certain half width. The ^{60}Co is usually used as an indicator for the set up procedure of the spectrum. In the data analysis, the resolution function can be described using mainly one gaussian as a good approximation to the prompt curve. The second gaussian was placed typically 30ps to the left of the main gaussian. The time resolution of the system (prompt curve) depends on the energy of the incident radiation, the type and the size of the detectors and on the performance of the timing discriminators. The energy dependency is due to the statistical effects; the higher the energy, the greater the signal and the smaller the statistical variation, roughly proportional to $(E)^{-1/2}$.

The most important contribution to the time resolution is from the time spread of the light pulse generated at different points in the scintillator since the time spread in the collection of this light on the photo-cathode of the PM, caused by the finite geometrical size of the scintillator amounts to $\sim$100ps. Once the scintillators and the PM are chosen, the next important factors in determining the time resolution of the system are the triggering of the fast discriminators and the settings of the single channel analyzer windows. Any increase in high voltage of the detectors may in some cases increase the time resolution. However, the setting of the windows strongly affects the FWHM. For ^{22}Na source, the FWHM and the relative intensities of the two gaussians are indicated in Table I for all the systems used in our laboratory. By decreasing the width of the windows, one can somewhat reduce the value of the FWHM, but this reduction would entail a reduction of the number of coincidences. Thus, choosing carefully the width of the windows can serve as a compromise between these two factors.

3.4.2 The time calibration

The time calibration, ie. the determination of the time difference between two successive channels in the MCA, was done by using one of the CFD's. The two outputs from the same CFD were connected to the TAC; one directly to the start input, the other via the delay to the stop input. By relating the channel number in which the very narrow peak that is obtained (width around one channel) positioned to the delay inserted, calibration is performed. The relation between delay and channel number is linear from 4 to 32ns (maximum delay), and the uncertainty of the time calibration is less then 1%. About 25-30 ps per channel is normally used.

3. 5. Analysis

The positron lifetime spectra are analyzed in terms of one or more exponentially decaying functions and a constant background all convoluted with the instrumental resolution function. The decay constants of the exponentials are the annihilation rates of the different possible

annihilation processes as determined earlier in section 3.4.

The spectra in this work were analyzed using the PC-version of a computer program developed by Kirkegard and Eldrup (31). The fitting program RESOLUTION was used to extract the information from the spectra. The program was modified such that a range of start channels situated at the sharply increasing portion of the lifetime spectrum (see Figure 3.5) could be prescribed in order to study the stability of the results for different choices of the start-channel of the analyses. Start channels were choosen in a range corresponding to 1% to 30% of the peak counts.

The resolution function is described by a sum of two Gaussians. For all the three spectrometers used in this work, the resolution functions could be described using mainly one Gaussian. The second gaussian was displaced typically 30 ps to the left of the main gaussian. The number of decay rates, or lifetimes, the number of gaussians in the resolution function, and the source correction is specified by the user. By least squares analysis the values and variance of the parameters are determined. The measured experimental data and the fitted guessed values spectra are compared and the deviation is expressed in the quantity "variance of the fit". We use the least-squares criterion, that minimizes :

$$\phi=\sum_{i}^{n} \omega_i \Delta_i^2 \qquad i=1,2,\ldots,n$$

the sum being extended over n measuring points ($n=_{\sim}450$). Δ_i are the differences between the measured count numbers and those predicted by the model. The weights ω_i are in principle arbitrary. In this work we use "statistical weighting",

$$\omega_i=\frac{1}{\sigma_i^2}$$

where σ_i is the standard variance of the count number at the i'th data point, which in our case equals the mean of the count number due to the Poisson statistics. The quantity :

$$\phi = Min \sum_{1}^{n} (\frac{\Delta_i}{\sigma_i})^2$$

obeys approximately the χ^2-distribution with n-k degrees of freedom, where k is the number of free parameters to be estimated. When n-k is large, as indeed is the case in our applications, it can be shown that (ϕ_{min}/n-k) is normally distributed with a mean value of 1 and should therefore serve as an indicator of the validity of the assumed model with standard deviation 1/2(n-k). In practical applications the standard deviation of the fits is ± 0.06. Experimentally obtained fits around 1.00 ± 0.06 are statically significant to within 70%.

The parameters to be fitted in our model are thus annihilation rates, λ_i, intensities I_i, channel number equivalent to time equal zero T_o, and background B.

CHAPTER FOUR

DEFECTS IN SEMICONDUCTORS

CHAPTER FOUR

4.1. Defect Properties

The properties of defects play an important role in determining the physical properties of most crystalline substances. They strongly influence the resistivity, the low-temperature thermal conductivity by scattering phonons, the electronic conduction and related properties of semiconductors by acting as donors or acceptors, and the optical properties of ionic solids by introducing electron states with optical transitions.

Another property of defects is the charge states which can be deduced from carrier concentration studies . When only one level is introduced, such a determination is made simple by observing the direction in which carrier concentration changes. However, since such a simple situation is not generally realized, it is usually necessary to make additional investigations.

4.2. Impurity in Semiconductor (doping)

Electrical properties are usually affected by small quantities of defects which introduce levels in the forbidden gap. For example, recombination of minority carriers in silicon can be substantially affected by 10^{10} defects/cm^3. The addition of boron to silicon in the amount of 1 boron - atom to 10^5 silicon atoms increases the conductivity of pure silicon by a factor of 10^3 at room temperature. The deliberate addition of impurities to a semiconductor is called *doping*.

When an impurity atoms is incorporated substitutionally each atom forms four covalent bonds, one with each of its nearest neighbours, corresponding to the chemical valence four. If an impurity atom of valence five, such as antimony, is substituted in the lattice in place of a normal atom, there will be one valence electron from the impurity atom left over after the four covalent bonds are established with the nearest neighbours. Impurity atoms that can give up an electron

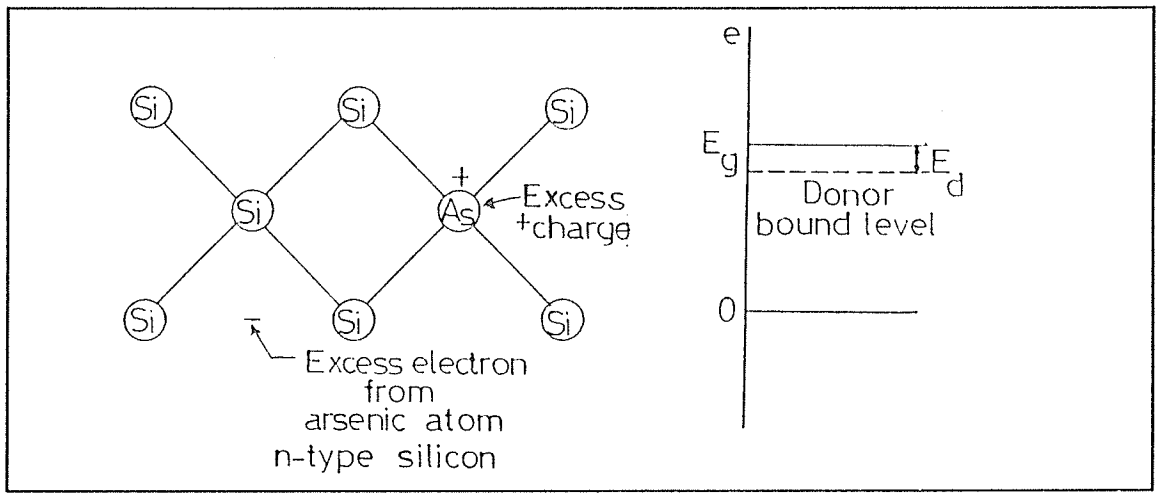

Figure 4.1: Charges associated with an arsenic impurity atom in silicon.

are called *donors* (see figure 4.1 Ref. 11).

The semiconductor can conduct in the impurity band by electrons hopping from donor to donor for light donor concentration. The process of impurity band conduction sets in at lower donor concentration levels if there are also some acceptor atoms present, so that some of the donors are always ionized. It is easier for a donor electron to hop to an ionized (unoccupied) donor than to an occupied donor atom, so that two electrons will not have to occupy the same site during charge transport.

A hole may be bound to a trivalent impurity in silicon (Figure.4.2 Ref.11) just as an electron is bound to a pentavalent impurity. Trivalent impurities such as B are called acceptors because they accept electrons from the valence band in order to complete the covalent bonds with neighbour atoms, leaving holes in the valence band. When an acceptor is ionized a hole is freed, which requires an input of energy. On the usual energy band diagram, an electron rises when it gains energy, whereas a hole sinks in gaining energy .

The donor and acceptor ionization energies in silicon are comparable with k_BT at room temperature (26meV), so that the thermal ionization of donors and acceptors is important in the electrical conductivity of silicon at room temperature. If donor atoms are present in greater

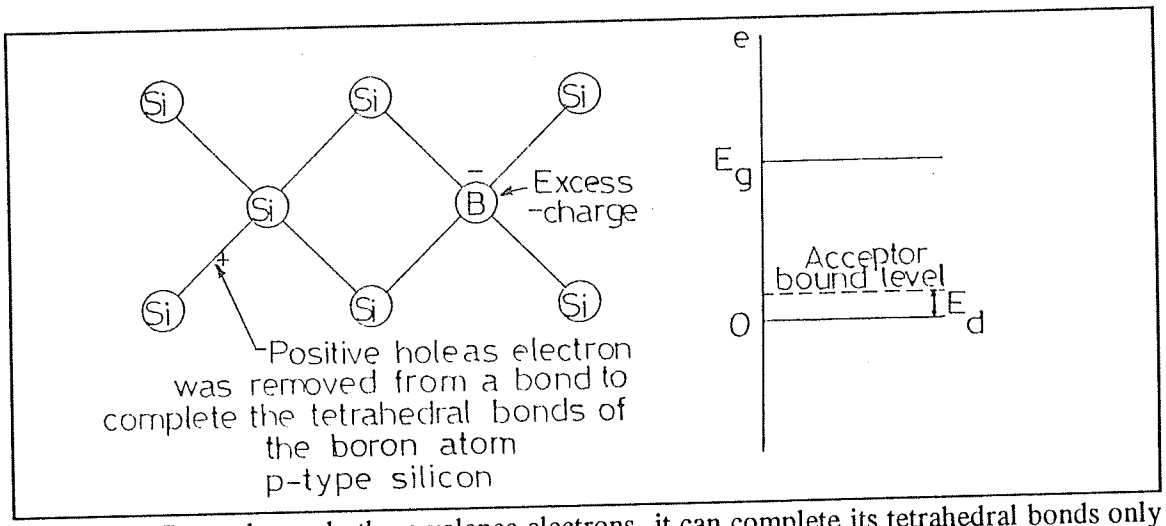

Figure 4.2; Boron has only three valence electrons, it can complete its tetrahedral bonds only by taking an electron from a Si-Si bond, leaving behind a hole in silicon valence band.

numbers than acceptors, the thermal ionization of donors will release electrons into the conduction band. The conductivity of the specimens then will be controlled by electrons (negative charges), and the material is said to be n-type.

If acceptors are dominant, holes will be released into the valence band and the conductivity will be controlled by holes (positive charges); the material is p-type. The sign of the Hall voltage is a test for n or p type.

The number of holes and electrons are equal in the intrinsic regime ie. in undoped, and defect free materials. The intrinsic electron concentration n_i at 300 K is 4.6×10^9 cm^{-3} in silicon. The electrical resistivity of intrinsic material is 2.6×10^5 Ωcm for silicon (32). Measurements of carrier concentration as a function of temperature is one of the methods to determine the position of energy levels introduced by defects into the forbidden gap. The slope of a logarithmic plot of carrier concentration versus reciprocal temperature has been used for energy level determination, but such a technique is susceptible to large error, and it is better to deduce from such a curve the point at which the defect level in question has a specific occupancy (33).

4.3. Geometrical Configuration of Point Defects

A point defect in a crystal is an entity that causes an interruption in the lattice periodicity. This occurs during the following circumstances.

a) An atom is removed from its regular lattice site, the defect is a *vacancy*.

b) An atom is in a site different from a regular (substitutional) lattice site; the defect is an *interstitial*. An interstitial defect can be of the same species as the atoms of the lattice (it is an *intrinsic* defect, the self-interstitial) or a different nature (it is an *extrinsic* interstitial defect).

c) An impurity occupies a substitutional site.

Various kinds of defects are also formed by the association of intrinsic or extrinsic, substitutional or interstitial defects. For instance, a vacancy close to a self-interstitial is a Frenkel pair; two vacancies on neighbouring lattice sites form a *divacancy*, etc. Schematic representation of simple point defects in a group IV semiconductor are shown in figure (4.3 Ref. 16) where the letters indicate: (a) vacancy; (b) self-interstitial; (c) interstitial impurity; (d) divacancy; (e) substitutional impurity; (f) vacancy-substitutional impurity complex.

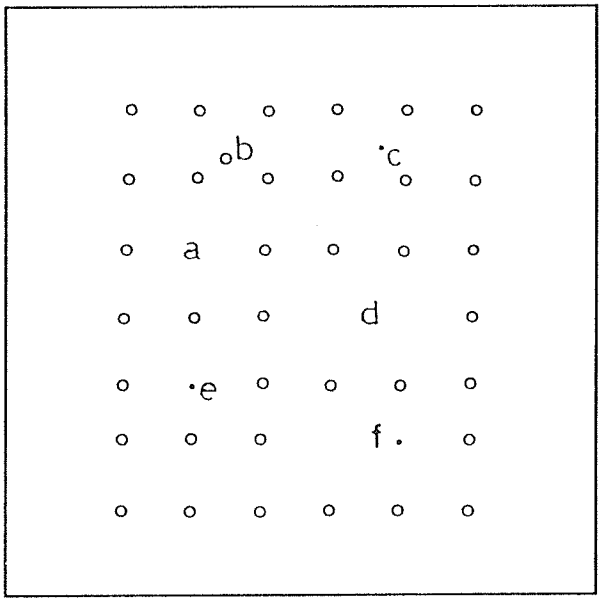

Figure 4.3; Schematic representation of simple point defects in a group IV semiconductor.

4.3.1. The vacancy

The lattice site of a missing ion or atom is called a vacancy also known as Schottky defect. Four bonds are broken in order to remove an atom from its lattice site and form a vacancy (Figure 4.4a Ref. 16). The broken (dangling) bonds can form new bonds which may lead to atomic displacements. This bonding

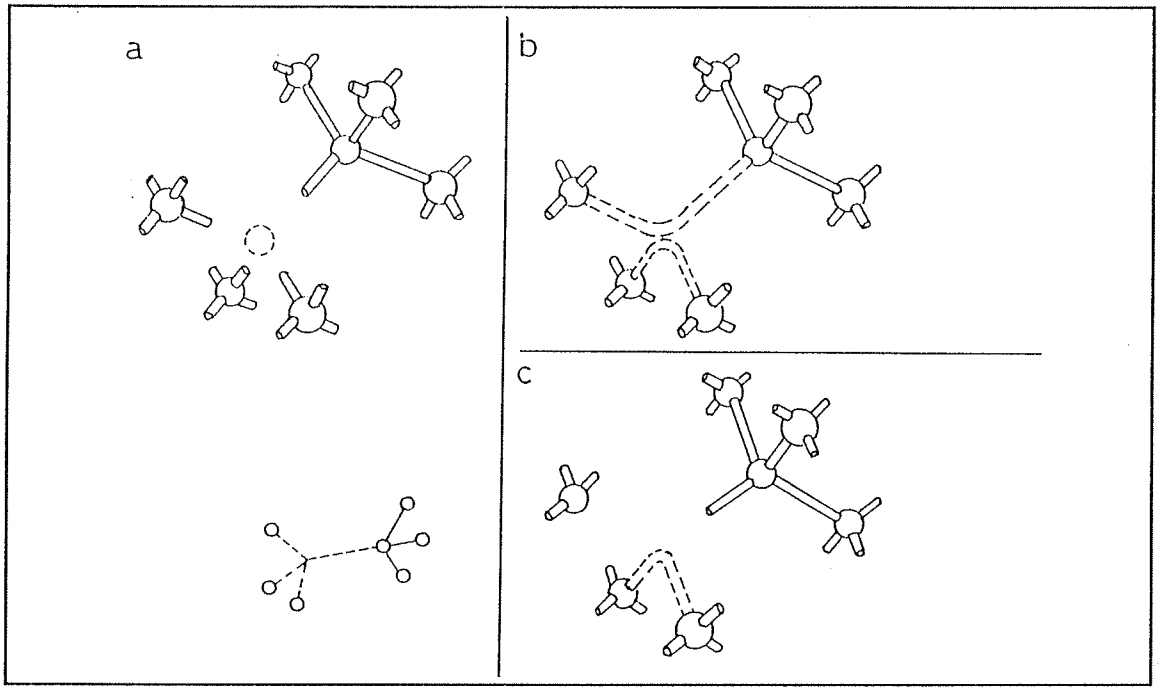

Figure 4.4a-c: The vacancy in diamond lattice. (a) Four bonds are broken to create it. (b) When there is one electron per dangling bond (V^o). (c) When an electron is missing (V^+).

depends on the charge state of the vacancy, i.e., on the number of electrons which occupy these dangling bonds (Figure 4.5b and c Ref. 16). In thermal equilibrium a certain number of lattice vacancies are always present in an otherwise perfect crystal because the entropy is increased by the presence of the disorder in the structure.

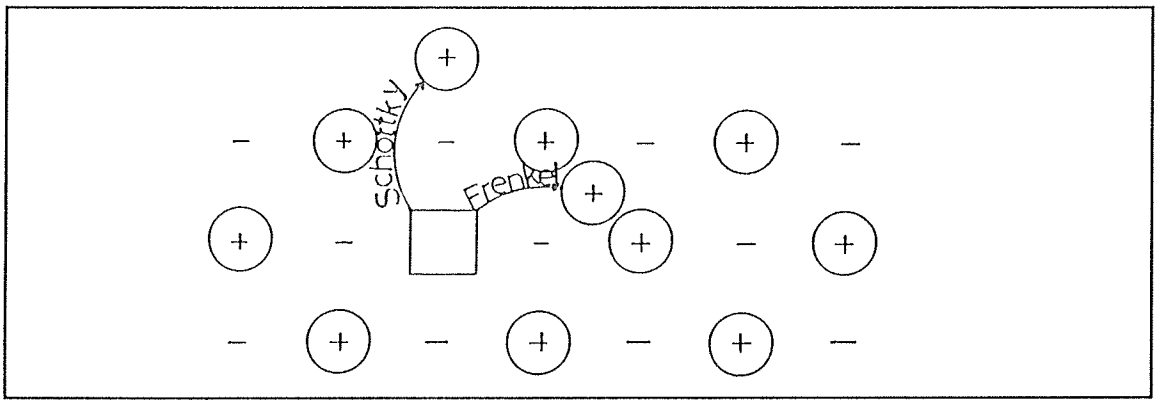

Figure 4.5: Schottky and Frenkel defects in an ionic crystal.

The equilibrium concentration of vacancies decreases as the temperature decreases. The actual

concentration of vacancies will be higher than the equilibrium value if the crystal is grown at an elevated temperature and then cooled suddenly, thereby freezing in the vacancies.

Another vacancy defect is the Frenkel defect (see figure 4.5 Ref.14) in which an atom is transferred from a lattice site to an *interstitial position*, a position not normally occupied by an atom.

4.3.2. The divacancy

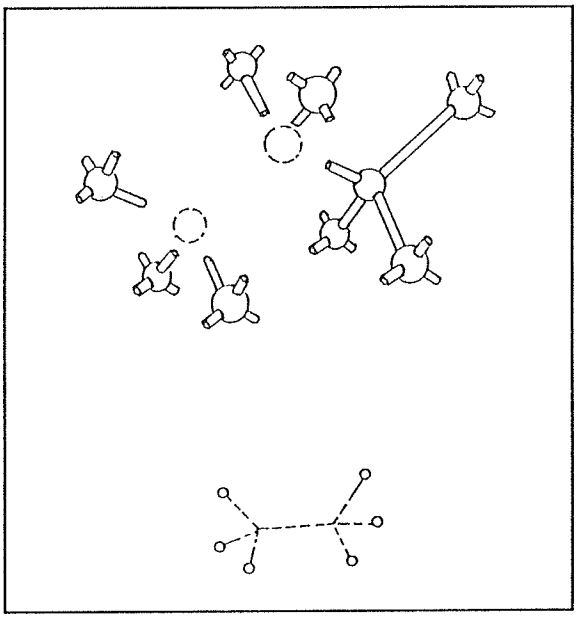

Figure 4.6; The divacancy configuration and its schematic two-dimensional representation.

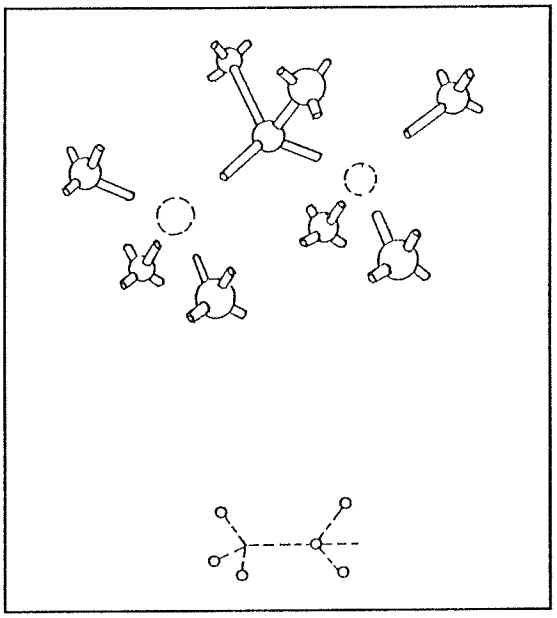

Figrue 4.7; The split-divacancy configuration and its schematic representation.

In many cases it is possible to produce groups of vacancies by prolonged radiation, heat treatment, or optical bleaching.

A divacancy consists of two nearest neighbour vacancies (Figure 4.6 Ref.16). The split-divacancy configuration, corresponding to the configuration of the divacancy in the saddle point for the migration, is given in Figure 4.7, (Ref.16).

4.3.3. The interstitial

When a lattice atom or ion is displaced from its normal site, it either returns to a normal site

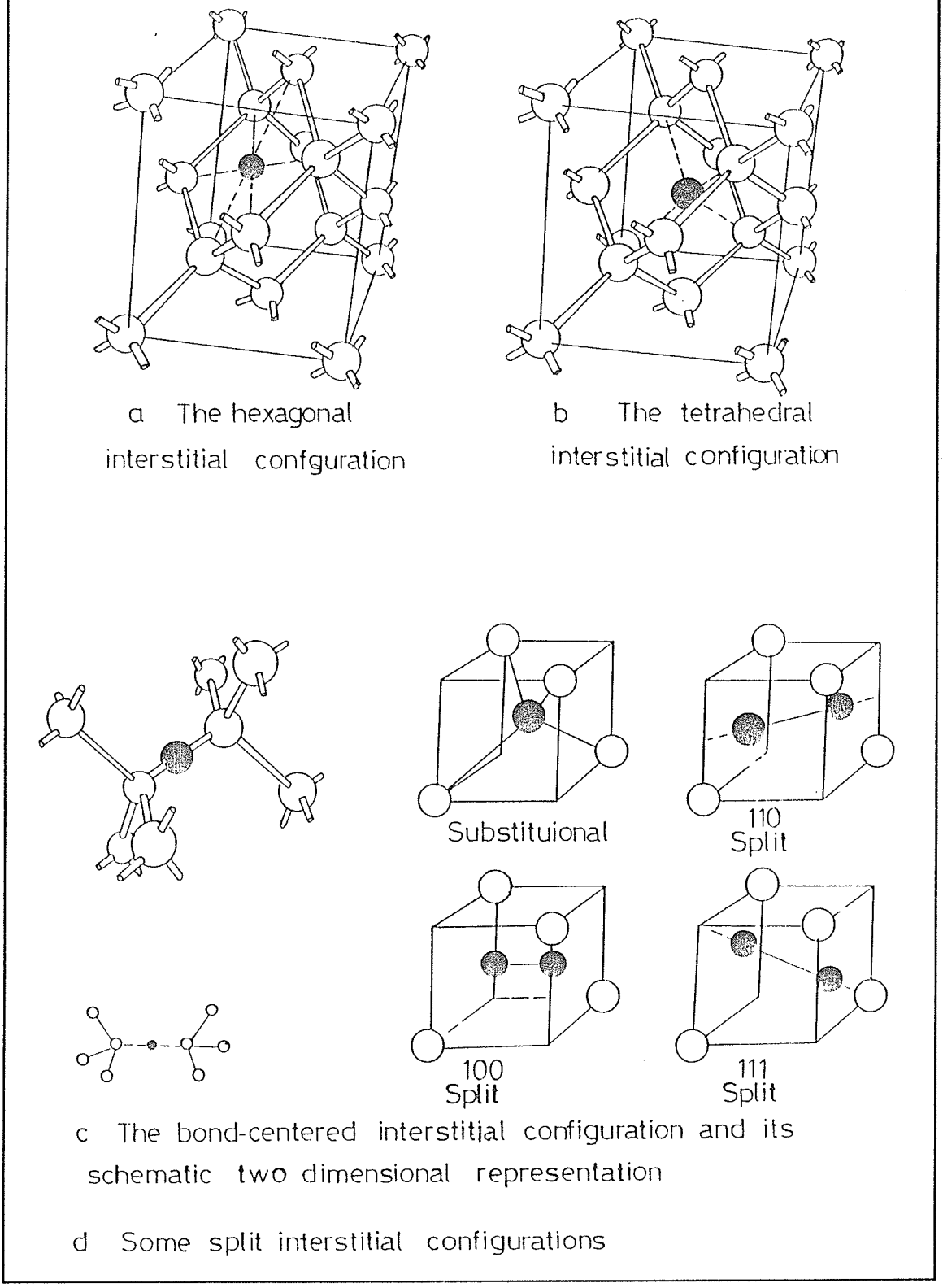

Figure 4.8 : Different intertitials configurations.

(annihilates), travels to a surface (a grain boundary or dislocation) or remains in a position that is not a normal lattice site. Such a position is refereed to as an *interstitial* site. The atom or ion is then an interstitial and the double defect consisting of the vacancy and interstitial is called the Frenkel defect. It is still not possible to decide what are the stable sites for an interstitial atom, but it is reasonable to consider that some of the high-symmetry sites are the stable interstitial positions. Because of the symmetry of the lattice, there may be several energetically equivalent positions per unit cell.

Two neighbouring locally stable interstitial sites are separated by other high-symmetry positions which correspond to saddle points of the electronic energy when all other atoms are again kept fixed at their perfect crystal positions. (The migrating path for interstitial will thus be from one stable site to another one through this saddle point position.) When the electron-phonon interaction is taken into account, it can give rise to distortions of the system. As a result the stable positions will no longer be those of high symmetry. These can be "off-centred" configurations in which the interstitial is slightly displaced from its ideal site. In this respect, once the ideal site has been identified, the situation becomes much the same as for the vacancy. Figures 4.8, b, c, and d (Ref.16) show different kinds of interstitial configurations.

Once again, the introduction of an interstitial induces a relaxation and a distortion of the lattice which surrounds it. The type of configuration the interstitial chooses depends on its ability to make any bonds with its neighbours and therefore can change with its charge state. Calculations have been done on these systems by the IBM group (34).

4.3.4. Complex Defects

When a simple defect moves, it can interact with other intrinsic as well as extrinsic point defects giving rise to a more complex defect. For instance, when the vacancy becomes mobile in silicon around 100 C or 200 C depending on the charged state, it can be trapped by an oxygen impurity

(present in Czochralski grown material) and form a V-O complex (the A centre), or by the doping impurity (B for instance) and form a V-B complex, or by another vacancy and form divacancies. Fig.4.9 (Ref.16) gives the configuration of the A centre in which the oxygen atom occupies a position slightly displaced from the substitutional vacancy site.

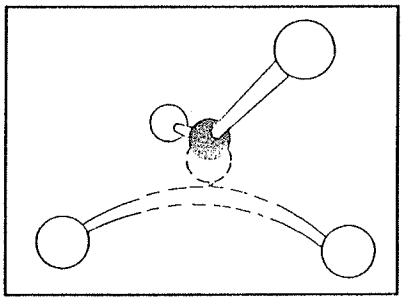

Figure 4.9; The A-centre configuration.

4.3.5. Aggregates

When the concentration of a particular defect is increased, they often tend to aggregate as the temperature is increased. Vacancies form divacancies that upon further heating becoming mobile or dissociating, form trivacancies, quadrivacancies and so on. In principle, the larger the number of defects involved in an aggregate, the larger the number of possible configuration (e.g., Figure 4.10 Ref.16) which gives one of the possible configurations for a penta-vacancy). But when the number of vacancies in the complex becomes sufficiently large, they tend to arrange themselves in voids, or form dislocation lops.

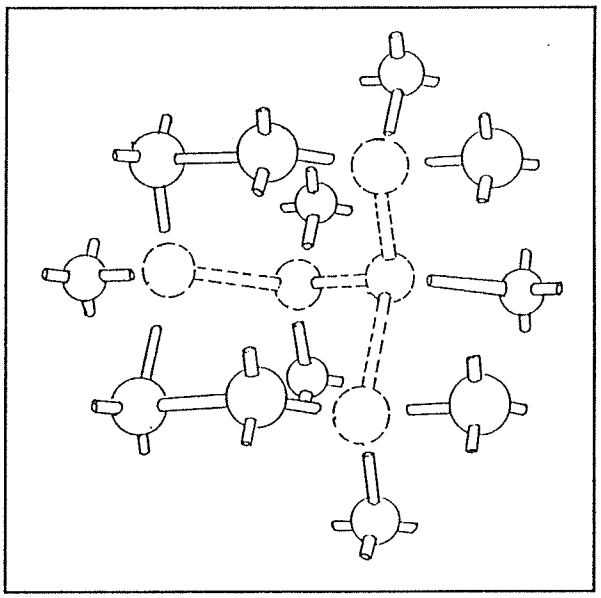

Figure 4.10; One of the possible configurations for a pentavacancy.

CHAPTER FIVE

AN OVERVIEW SURVEY OF PREVIOUS MEASUREMENTS IN SILICON

CHAPTER FIVE

5.1. Brief Historic survey of the Experimental Results in Silicon

A number of investigations have been carried out regarding the study of defects in silicon. These include studies of the electronic properties of vacancies V, divacancies V_2, and interstitials I as well as of the formation energy E_F, migration energy E_m, and divacancy binding energy E_2 (V_2) (35-40). These calculations range from model calculations and Morse calculations, to band structure and molecular orbital treatments. In many instances, the early calculations had only a limited validity, but increasing sophistication is resulting in a closer and closer coordination between experiment and theory. The properties of a few defects are well established experimentally.

Watkins made experimental observations by means of electron paramagnetic resonance on the V^+ and V^- states in silicon and indirect measurements on the properties of V^o (41).

A number of vacancy-related defects configuration has been well established by EPR

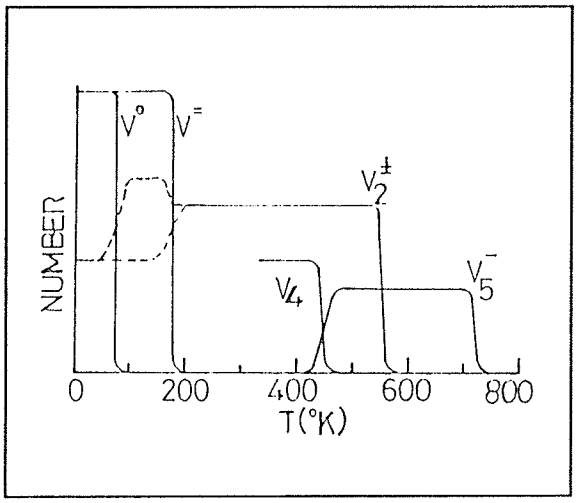

Figure 5.1; Schematic representation of the recovery stages of various vacancy-related defects in silicon.

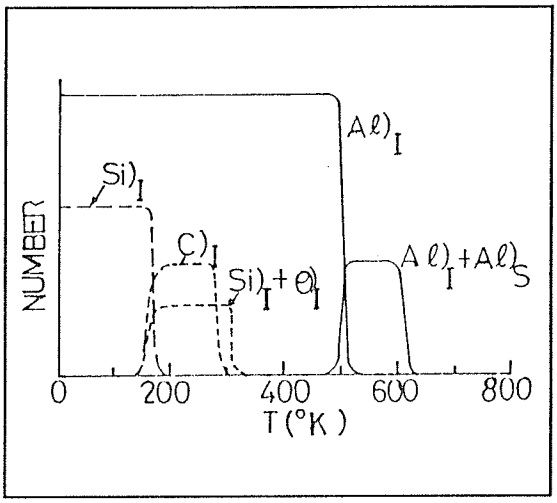

Figure 5.2; Schematic representation of the various recovery stages of interstitial-related defects in Si.

measurements in silicon [V^- and V^+], [V_2^- and V_2^+], V_4, V_5, (V+Sb), (V+B), and (V+O) (42-49). There is also evidence of (V+C) and vacancy aggregates with oxygen impurities. Figure 5.1 (Ref.151) shows schematically the temperature dependence of the recovery of these defects. Figure 5.2 (Ref.151) shows what is known of the recovery of interstitial-related defects in silicon.

In n-type material Watkins observed a spectrum which he tentatively attributed to the silicon interstitial; the spectrum disappears at approximately 170 K. Other workers (50-53) have found the formation of infrared bands at this temperature which they attribute to an interstitial carbon atom and/or to an interstitial silicon associated with an oxygen atom, as shown in Fig.5.2 (No interstitial vacancy pairs have been observed in silicon).

About 1959 Brown, Augustyniak, and Waite (54) demonstrated the sensitivity of defect annealing to dopant impurities while Watkins, Corbett, and Walke, together with Bemski (55), showed the effects of oxygen on electron spin resonance in silicon. Early positron lifetime measurements on silicon (56-58) showed that the mean lifetime changed upon irradiation but that effects from doping seemed less certain (59,60). Dannefaer *et al* (61) determined specific lifetimes for vacancies in neutron irradiated Si for the first time and Fuhs *et al* (62) investigated 1 MeV electron irradiated Si at low temperatures where they succeeded in observing the monovacancy. These measurements provided the basis for identifying lifetimes with specific defects, and they also indicated that the positron trapping cross-section may be strongly temperature dependent by virtue of negative defect charges (63).

Another interesting, and important, lifetime was found by Kelly and Lambrecht (64) who detected a very short lived component ($\approx$60 ps) in Czochralski grown silicon (Cz-Si), i.e. silicon which is contaminated with oxygen to a typical concentration of 10^{18} cm^{-3} (20 ppm). Such a short lifetime has not been observed in float zone refined (Fz) silicon where the oxygen concentration

is only about 10^{16} cm^{-3} or less, thus indicating that the growth process of the silicon itself is of importance in positron experiments. From EPR, IR, and resistivity measurements we already know that oxygen has profound effects on other defects (65). These early lifetime measurements have probably identified some of the important issues and differences compared to metals.

We must expect much more complex systems, largely due to the fact that defects may have a net charge. The monovacancy can exist in 5 differently charged states +, + +, 0, -, -- (see Fig. 5.3), so that positrons may "miss" entirely the presence of monovacancies if they are positively charged, i.e. when the Fermi level is below E + 0.1 eV. For Fermi levels above this value, we would expect to observe monovacancies in the neutral or negatively charged states, and we would expect that, when in a negative charge state, the positron trapping cross-section would decrease strongly with increasing temperature, something like T^{-n}, n = 2 to 3 (66). It should be emphasized that this temperature dependency also constitutes a simple check as to the net

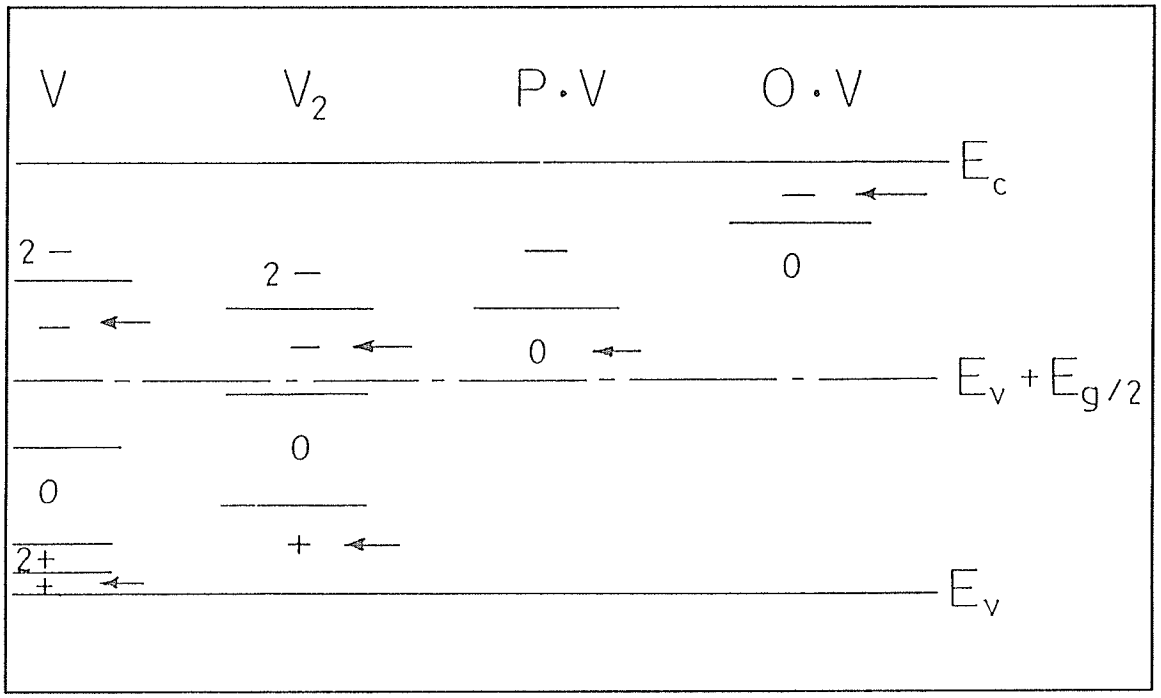

Figure 5.3; Energy levels for charged states of different types of defects in Si at low temperatures. The arrows indicate EPR active charge states.

charge state of any observable defect, not only the monovacancy. This is very valuable information for defect identification. One pitfall in such experiments is that they can be obscured by the fact that the Fermi level moves with temperature so that the relative population of two charge states may change significantly, thus bringing about a strong deviation from the T^{-n} dependency of trapping rate.

The very fact that monovacancies can exist in various charged states and that they migrate at low temperatures (70 to 170K) (67) makes possible strong interactions with common impurities such as shallow donors/acceptors, oxygen and carbon in Cz-Si. Prominent examples are phosphorus-vacancy pairs (E-centre, stable to at least 150 C), (68) boron-vacancy pairs (stable only up to 260 K) (69) and oxygen-vacancy "pairs", the A centre, stable up to 300 C (70). The latter complex is actually a substitutional oxygen atom created from the normal interstitial oxygen by absorption of a monovacancy. These complexes have their own energy levels in the band gap (see Fig.5.3). Apart from the vacancy-type defects it must also be expected that acceptor-like defects without associated vacancies are positron traps at least at low temperatures, that is they are shallow traps. Positrons could be trapped around the negatively charged state of the A-centre yielding a lifetime close to the bulk lifetime. This significantly complicates any type of analysis. At low temperatures such effects may well be overwhelming and leading to complete trapping in shallow states---a situation which resembles carrier freeze-out in semiconductors. The binding energy would be at shallow acceptor levels, i.e. about 20 meV.

From the wealth of possible defect charges and reactions, some new and fundamental problems are encountered. Is there a charge dependent positron lifetime for a given defect? It is of course of no practical interest if the change is a few picoseconds, but if larger ($\approx$ 10-30 ps) this may interfere with other lifetimes. How does the trapping cross-section change with the state of charge? This has immediate importance for defect concentration estimates in heavily doped Si

where few EPR data are available, and is of importance when assessing concentrations of originally electrical inactive defects. Shallow traps are definite possibilities and may well play a role even for room temperature measurements.

5.2. An Overview of Oxygen in Silicon

Oxygen in silicon is an important scientific and technological subject. It derives its technological importance from the fact that silicon crystals pulled from silica crucibles are very inexpensive and, therefore, have been the standard substrates for fabrication of integrated circuits. The scientific interest originates from the wide variety of phenomena that occur when cooled Czochralski (Cz) Si crystals become supersaturated with oxygen.

The growth phenomenon is described schematically by the dashed line marked "G" in Figure 5.4 (Ref.152). The Si melt is in contact with an SiO_2 crucible and the growing Si crystal, and oxygen is transported mainly by convection from the crucible surface to the growing crystal interface. Some success in adjusting the oxygen concentration and homogeneity in Cz Silicon has been achieved by using magnetic fields in stabilizing the melt convection patterns. The phenomena involving oxygen in Si are schematically superimposed on the Si-O phase diagram in Figure 5.4. Three broad categories of oxygen behaviour can be identified. First, there is the intrinsic

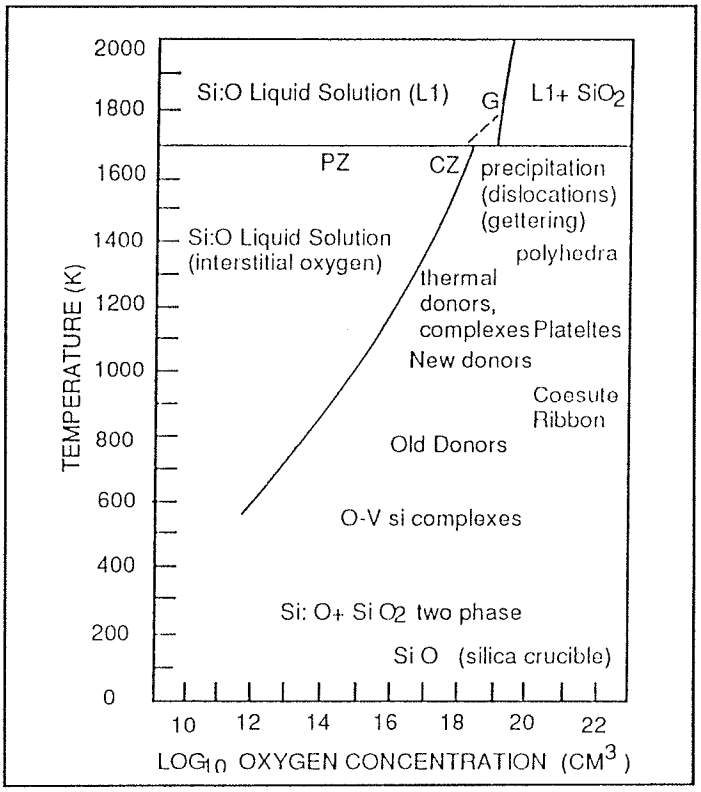

Figure 5.4; Schematic representation of oxygen related phenomena superimposed on the Si-O phase diagram.

behaviour of dissolved oxygen within the equilibrium Si:O solid solution, such as diffusivity and solubility. Second, there is the non-equilibrium (metastable) oxygen containing structures involving the supersaturated Si:O solutions, such as *thermal donors* and O-V_{Si} complexes. Third, there is the thermodynamically stable oxide precipitates, whose shape and structure depend on their surface energy and related defect production. Dislocations and gettering are closely associated with precipitation. Dislocations are nucleated by precipitates but can be pinned by interstitial oxygen. Strain and defects surrounding precipitates can attract metallic impurities (gettering).

Oxygen can interact with *point defects* in two different ways. The first is the low temperature complexing of interstitial oxygen with vacancies e.g., the O-V_{Si}, *A-centre*. If the reaction is followed by the capture of a Si interstitial, an accelerated hop of the oxygen atom might occur. A second type of oxygen-point defect interaction is the generation of point defects, especially Si interstitials, during thermal oxidation and precipitation of excess oxygen. The precipitation behaviour is governed by interstitial oxygen concentration and annealing temperature and thermal history. The most controversial topic of the oxygen phenomena is, arguably, the thermal donor formed at 450 C. This is generally presumed to involve an oxygen complex. Although the thermal donor formation kinetics have been studied for decades and many of its electrical and optical properties have been determined, its structure is still a mystery. In addition, a new thermal donor produced at higher temperatures may also be related to oxygen. Microscopic aggregation of oxygen and point defects is certain to occur during cooling of the crystal from the melt, as evidenced by the typical formation of thermal donors.

Although commercially-grown Si crystals are quite perfect solids, it is important to realize that Cz wafers generally are not ideal thermodynamic systems for studying the complex behaviour of oxygen in Si. The thermal history of the crystal is determined predominantly by the thermal

gradients, cooling rates, and other production growth procedures, and this thermal history varies with position in the crystal. Annealing of Cz crystals to achieve a reproducible thermal history and a uniform distribution of oxygen within the crystal has several disadvantages. The first is the possible introduction of metallic impurities from as-polished surface contamination and wafer handling. The second disadvantage is that a protective coating is required to prevent out diffusion of oxygen to the Si surface. Thirdly, in order to specify the new thermal history, it is necessary to control, or at least monitor, the cooling rate. Unfortunately, the detailed impact of thermal history (and ambient) on the equilibrium and kinetics of point defects is unknown.

Prolonged heat treatment at 450 C of oxygen rich silicon gives rise to up to $3x10^{16}/cm^3$ shallow donors (71). Resistivity measurements showed that the initial formation rate was proportional to $[O]^4$ and that the maximum concentration was proportional to $[O]^3$. Infrared measurements (72) show that the oxygen donor is a double donor and that it is a family of complexes. EPR and IR absorption measurements show ground state splitting that can be understood in terms of an effective mass, like ground state, that is constructed from wave functions associated with a single pair of conduction band valleys. ENDOR measurements (73) are in agreement with the effective mass theory picture of the donor that has been developed and have the potential to provide detailed structural information about the individual donor species. Based on the TEM observation of ribbon-like structures formed for low temperature anneals, several groups have suggested that the family of oxygen donor complexes are chain-like structures extended along [110] directions (74). Oxygen atoms are added to the defect to give rise to the family of donor species. Several clusters have been suggested for the electrically active portion of the thermal donor. Theoretical calculations have been performed to determine the relative stability of several oxygen related species and their electronic properties (75). It has also been shown that the trend in thermal donor ground state energies can be fitted by a model in which a repulsive potential (76) is added

to the Coulomb potential. The repulsion increases as oxygen atoms are added to the growing defect in this model.

Donor models that only include oxygen share a common problem. Such models require an oxygen diffusivity that is several orders of magnitude larger than has been measured. It had been hoped that anomalous diffusion might alleviate the problems in kinetic models, but further studies show that enhanced oxygen diffusion does not provide a simple solution. It is now believed that the mechanism for anomalous oxygen diffusion involves silicon vacancies (77). New results have been reported for the loss of interstitial oxygen during oxygen donor formation (78,79). In these studies it is shown that the oxygen loss can be attributed to the formation of oxygen dimers. The dimerization reaction is consistent with ordinary oxygen diffusion and a 5 to 10 Å capture radius. If the same model is used to calculate the concentration of higher order complexes, then these concentrations are orders of magnitude too small to explain the hierarchy of donor complexes (80). It is still not clear why higher order complexes should involve enhanced diffusion when the dimerization does not. Several oxygen donor models have been suggested that include components other than oxygen, The most recent suggestion (81,82) is that the Si interstitials are ejected as oxygen dimers are formed in an aggregate to produce the electrically active donor species. The interstitials might be nucleated at some other defect site, perhaps upon oxygen dimers or trimers. In such a scheme the oxygen portion of the defect is small so that the oxygen diffusion constant might be consistent with the formation kinetics. The fast diffusing Si interstitials would be responsible for the evolution of the donor complexes for continued annealing. Models that involve Si interstitials are at a very early stage of development as compared to "oxygen only" models so that it is difficult to asses whether the formation kinetics and other physical properties of oxygen donors can be explained consistently.

Even after its 30 year history, research in the oxygen donor problem continues to be fresh and

exciting. New results and ideas continue to stimulate further investigation into the most basic questions about the oxygen donor's structure and formation.

The research of the past few years has yielded a unique, fundamental understanding of the behaviour of oxygen in silicon. The oxygen donor centre plays an active role in a rich array of phenomena. *Formation kinetics* portray a diffusion limited aggregation of a four oxygen cluster. The misfit of quantitative rates with theory suggests that further work is necessary in the accurate determination of the absolute oxygen concentration with micrometer resolution. The electrical activity of the donor and its participation in the early stages of oxygen aggregation qualitatively account for the enhancement of precipitation in p-type material and the retardation in n-type material.

5.3. An Overview of Carbon in Silicon

Around the time that silicon was first analyzed to determine its oxygen content, related measurements were carried out which suggested that carbon impurity might also be present in a high concentration of up to 10^{19} atom cm^{-3}. It is almost certain that such high estimates exceeded the true concentrations, most likely because of contamination introduced during the analytical procedures adopted, but nevertheless they stimulated research on the topic which is continuing to the present day.

Later, Newman and Wakefield (83) showed that heat treatments of single crystal silicon in vacuum produced surface coatings of cubic β-silicon carbide particles which were detected by reflection electron diffraction and electron microscopy using extraction replica techniques. These observations could be explained by invoking a chemical reaction between the silicon and organic contamination in the ambient. However it was pointed out that it was necessary to consider the possibility that carbon dissolved in the silicon could have diffused to the external surface to contribute to the carbide formation. Quantitative estimates of this process were not possible

because neither the carbon content of samples nor the diffusion coefficient of carbon were known. Work by Hall (84), Dash (85) and Scace and Stack (86), indicated that silicon crystals might contain up to 10^{18} atom cm^{-3} of the impurity. The dissolution of SiC into an oxygen-free silicon melt led to an estimate of the solubility of carbon in the liquid of about $3x10^{18}$ cm^{-3}, and it was assumed that the segregation coefficient might be around 0.3. It was imperative to gain further information. As a next step, it was shown by Newman (87) using electron diffraction techniques applied to specially etched and doped crystals that precipitated particles of β-SiC could also grow along the cores of grown-in dislocations during heat treatments at 1150°C. If the carbon had diffused from the surrounding matrix it was again implied that the concentration would have had to be close to or even greater than 10^{18} cm^{-3}, but it was still not clear whether the carbon was originally in the solution or whether it had diffused in from the external surfaces. To resolve this uncertainty Newman and Wakefield (88) measured the diffusion coefficient by diffusing carbon into monocrystalline samples from a surface coating of SiC enriched with the ^{14}C isotope. These treatments were carried out in silica tubes so the system would have been saturated with oxygen. A combination of the measured values of diffusion coefficient (D) and an estimated solubility of 10^{18} atom cm^{-3} led to the conclusion that the grown-in impurity could indeed diffuse to an external surface to produce a measurable growth of SiC. This turns out, however, to be a slow process and heating at 1250°C for 24 hours would produce a coating equivalent in thickness to about only one mono layer.

It is important to include the contribution of Baker et al (89) who measured the carbon contents of samples using the infrared technique and then made careful X-ray measurements of the lattice parameter a_o of the same samples. It was shown that a_o decreased as the concentration of carbon increased, thus confirming that small carbon atoms occupy substitutional lattice sites in as-grown material. Due to these findings, it is now a routine matter to obtain maps of the carbon content

via X-ray topography made from wafers of silicon grown by the float zone (FZ) technique. Unfortunately, the presence of interstitial oxygen in Czochralski (Cz) material leads to an increase in a_o (90) so that X-ray measurements do not give unambiguous data if both impurities are present in comparable concentrations. A similar problem also exists for small dopant atoms such as boron.

5.3.1. Carbon in As-grown Silicon

Carbon atoms have a lower mass than silicon atoms and give rise to a localized vibrational mode (LVM). ^{12}C gives a mode at 607 cm^{-1} and modes at 589 and 573 cm^{-1} arise from ^{13}C and ^{14}C respectively (91,92). They are in isotopically enriched crystals and in good agreement with the theory of Dawber and Ellott (93). There is a relatively smooth sequence of frequencies with the two substitutional boron isotopes $^{11}B^-$ and $^{10}B^-$ which give modes at 623 and 646 cm^{-1} (94). It is implied that the force constants between the two types of impurity and their four nearest neighbour silicon atoms are similar thus giving evidence that carbon occupies substitutional sites. The frequencies quoted are for a sample temperature of 77 K and they should each be reduced by some three wave numbers for a sample temperature of 300 K.

There is also evidence that the presence of a high concentration of dissolved oxygen in a sample enhances the solubility of carbon. There could be important consequences in relation to oxygen precipitation in Cz crystals. There are strongly polarized views on this matter, one being that carbon plays an important role in the process and the other which suggests that carbon is unimportant.

In Cz silicon, carbon-oxygen complexes have been found in as-grown samples. Modes at 589, 640 and 690 cm^{-1} were attributed to the vibrations of the complex carbon, while there was a modified vibrational modes of oxygen at 1104 cm^{-1} (95). When ^{13}C is present the "carbon" modes shift to lower frequencies confirming the involvement of the impurity. No detectable

splitting, however was found for the "oxygen" mode. The defect complex must have a low symmetry but no atomic model has been determined. A related [C-O] complex with a lower concentration is sometimes present giving an "oxygen" mode at 1052 cm^{-1} and carbon modes at somewhat higher frequencies than for the first complex. Again no atomic model exists for this centre (96).

5.3.2. Effects of Heat Treatments

Heat treatments may be conveniently divided into two categories. There are those at high temperature ($T > 1000°C$), where substitutional carbon can migrate and those at low temperature ($T \approx 450°C$) where this process could not occur because the diffusion coefficient is too small. High temperature treatments of FZ silicon containing carbon often appear to have little effect on the amount of the impurity which remains in solution, unless dislocations are present, or nucleation sites are provided by a prior heat treatment or irradiation (97). When interstitial oxygen atoms precipitate, self-interstitials have been proposed to be generated to accommodate the local increase in volume (98). If carbon atoms co-precipitate, the process of producing space by emission of self interstitial would be greatly diminished because of the small size of the carbon atom. It was not therefore surprising that SiC particles formed around dislocation lines where SiO_2 particles had nucleated (99). It may be that the aggregation of oxygen atoms occurs first, leading to the generation of self-interstitials even at these very high temperatures. These defects would be trapped by the carbon atoms which could then diffuse at a very high rate.

The precipitated silicon carbide was also detected by IR absorption but the band appeared at 12.2 μm rather than 12.6 μm and was very much broadened (100). These effects occur because of the small size of the SiC particles and the fact that they are embedded in the silicon matrix. As a concluding remark, the presence of the carbon originally at a level of 2×10^{18} atom cm^{-3} had no detectable effect on the solubility data obtained for the oxygen.

When CZ crystals are heated at 450°C, there is generation of thermal donors up to concentrations of $\sim 10^{16}$ cm^{-3} after heating times of about 100 hours. However, this concentration is reduced when a high concentration of carbon is present (101,102). In early research, absorption from carbon-oxygen clusters was observed and it was inferred that a fraction of the carbon had been transferred to interstitial sites because of the similarity of the LVM absorption produced in irradiated silicon (103). Recently, it was demonstrated that there was a loss of substitutional carbon with time of heating which correlated with the loss of oxygen (104). Using the argument that the rate of carbon loss was equal to the rate at which self interstitials were trapped, it was deduced that in material containing a high carbon content (10^{18} cm^{-3}) essentially all the self-interstitials were trapped by this means. Now, thirty years after the first measurements, the assignment of oxygen clusters to the thermal donor centres has been questioned (105). It has now been suggested that aggregates of self-interstitials might be the defects responsible for donor activity. If this is true, such defects should not form in heavily carbon-doped silicon and the inhibiting effect on the thermal donor formation from the presence of carbon could be explained. Further investigation is needed on this rather radical suggestion concerning the nature of the thermal donor.

It would appear that current research in carbon relates primarily to the fact that the substitutional impurity can selectively trap a mobile self-interstitial. This process occurs at temperatures at least as low as 77 or as high as 773 K. Further work is required to see how far these limits can be extended. It is important therefore to have an absolute calibration for the 607 cm^{-1} LVM band so that measurements of the removal of carbon from substitutional sites are quantitative. Carbon interstitials may be produced by surface diffusions, internal oxygen aggregation, or high energy irradiations by ions, neutrons or electrons.

Precaution has to be taken if samples contain other impurities such as boron which is also an

efficient trap for self-intersitials and competes with the carbon in this respect.

5.4 Positron lifetimes

Fuhs et. al. (106) for the first time in 1987, determined that positrons are trapped by monovacancies in electron irradiated silicon at 20 K by EPR. Table I lists some of the established lifetimes for the aggregates of vacancies determined by other researchers. It appears that as the size of the vacancy aggregate grows larger and larger, the positron lifetimes increases to approach a theoretical limit of 500ps for large aggregates (voids).

Table I. Positron Lifetimes for Various Vacancy Aggregates.

	Bulk	V_1	V_2	V_4	V_5	V_6(?)
τ(ps)	218	266-270	266-270	390-450	480-520	>520
Ref.	(146)	(62,146)	(120,62)	(120)	(47)	(123)

Soon afterwards, Dannefaer et.al. (107) had shown by means of positron annihilation technique that all the main defects in electron irradiated Cz-Si can be detected, and the correlation between EPR and positron annihilation, as well as with independent theoretical calculations of positron lifetimes are significant for the physical interpretations of lifetime values.

Table II lists positron lifetimes and trapping cross sections for various defects in silicon. Included are the temperature ranges in which trapping cross sections were determined. The data listed in Table II are mainly based on the experimental results conducted on electron irradiated Cz-silicon samples.

The data in Tables I and II provide the key information regarding lifetimes which can be used to identify the defect type, and trapping cross section. The temperature dependency of the

trapping cross-section is also used to establish the charge state of the defect. Defects which are positively charged cannot be detected by positrons.

Table II. Positron lifetimes, τ, and trapping cross section σ, for various defects in silicon.

Defects	τ(ps)	σ(cm^2)	Temp. Dependence	Temp. range(K)
V^o	?			
V^-	270 ± 5[1-3]	$2x10^{-12}$-$1x10^{-11}$	$T^{-3,1}$	$60<T<120$
V^o2	320 ± 5	$\sim 10^{-15}$@300K[4]	T^o	$30<T<300$
V^-_2	325 ± 5	$\sim 4x10^{-15}$@..	$\sim T^{-2,5}$	$70<T<300$
V^{--}_2	325 ± 5	$\sim 8x10^{-15}$@..	$\sim T^{-2,5}$	$30<T<300$
V_2O^o	270 ± 5	$\sim 10^{-15}$@..	T^o	$30<T<300$
$VO^o(A^o)$	?			
$VO^-(A^-)$	225 ± 5			
$P.V^o(E^o)$	?			
$PV^-(E^-)$	248-265	$3x10^{-14}$@20K[3]	T^o	$20<T<150$

1: Ref. (62), 2: Ref. (146), 3: Ref. (148), 4: Ref. (134), 5: Ref. (120)

CHAPTER SIX

EXPERIMENTAL RESULTS AND DISCUSSION

CHAPTER SIX

Chapter six is designated to the findings of the experimental investigations which were performed at the university of Winnipeg positron laboratory - Winnipeg - Manitoba - Canada.

The chapter is organized in the following manner: First an introduction is given to thermal donor formation as well as to the heat-treatment induced defects in Cz-silicon. Then the chapter is divided into three sections. In the first section we report the defect characteristics that can be detected across a given wafer. In the second section we discuss the heat-treatment induced defects in Cz-silicon. The third section deals with the effects of oxygen interstitials and carbon impurities on thermal donors kinetics.

6.1 INTRODUCTION

It is well known that the main impurities during the cool-down of Czochralski-grown silicon ingots are oxygen atoms. Since Kaiser *et al.* (108) first presented in 1958 the so called KRF model that describes the formation of thermal donors (TD's) in silicon, oxygen in silicon has been under continuous investigation. The concentration of oxygen atoms is far above the solid solubility at room temperature, so we can expect that various precipitates of oxygen atoms would be present in Cz-silicon specimens. These oxygen atoms play an important role in affecting the electrical and the mechanical properties of the silicon wafer. The major interest in studying the behaviour of oxygen in silicon is related to the fact that oxygen considerably influences the fabrication of electronic devices.

During the growth process of Cz-silicon ingots, several types of defects may be formed. One type of these defects is the oxygen interstitial. However, after subsequent heat-treatments, some

oxygen aggregates and thermal donors (TD's) may be induced at temperatures above 400 C (109,110). These donors, formed after several hours of annealing at 450 C, have been argued to arise from agglomeration of about four interstitial oxygen atoms [O_i]. Furthermore, the formation kinetics of the thermal donors is strongly influenced by carbon impurities (111-113). At an early stage, it was recognised that the equilibrium diffusion of the oxygen would have to be enhanced by about an order of magnitude to explain the observed kinetics.

Many of the techniques usually employed to investigate the structure of defects in semiconductors, such as hyperfine magnetic resonance method and local mode vibration investigations, do not yield information on other *grown-in* defects in Cz-silicon. The method of electron nuclear double resonance (ENDOR) has been used by other workers to demonstrate the presence of oxygen in thermal donors in silicon (114). Experimental investigations of impurity centres containing two oxygen atoms have been made by a variety of methods (115-118). Calculation of electron structure and geometry of a VO_2 (vacancy+O_2) complex were first made by the semi empirical method (119). By using the positron annihilation technique, Dannefaer *et. al.* (120-126) reported systematic study of vacancy-type defects in Si specimens and demonstrated that the positron annihilation technique can be used as a microscopic tool for vacancies and their various agglomerations. Dannefaer also reported that positrons can be trapped by interstitial oxygen clusters and the lifetime of positrons trapped by such defects (100 ps) is shorter than that of positrons annihilated in the bulk (218 ps) in Cz-Si specimens (127,128).

6.2 DEFECT CHARACTERISTICS ACROSS SILICON WAFERS

It is generally accepted that point defects play an important role in the precipitation process as evident by a multitude of observations of oxygen-defect complexes after heat treatment (129). As a consequence of the cool-down of the silicon crystals grown by Czochralski (Cz) method,

oxygen precipitation occurs, both homogenously and inhomogenously. Previous investigations were done by Dannefaer *et al.* (130) where it was found that significant differences in the defect characteristics can be detected across a given wafer and that heat treatment can give rise to interesting impurity-defect complexes, at least at a transient level (131).

6.2.1 Samples

The wafers investigated here were p-type material with resistivity $\sim$10 Ωcm. Four sets of wafers were investigated, set I cut from a boule grown under standard pull speed (0.85mm/min), set II from a boule grown under medium pull speed and set III from a boule grown under fast pull speed (1.26mm/min). The interstitial oxygen concentration $[O_i]$ for the for sets is around 10^{18} /cm^3.

These measurements were preformed at four different locations across the wafer starting at 0.5cm from the edge of the wafer and increasing by an increment of 2cm towards the centre of the wafer. All the experiments were conducted at room temperature.

6.2.2 Results

Figure 6.1 shows the lifetime data for four different wafers which were grown at different pull speeds as a function of the measurement position. For most of the points plotted in this figure, the average of two measurements are shown. Only for the standard pull speed the points reflect the results for single measurements. The results exhibit a statistical scatter of 20ps and they lie within the lifetime range of the monovacancy (270ps) and the divacancy (325ps). Only the medium pull speed sample showed a higher lifetime value of 335ps at the centre of the sample. The trapping rate in Figure 6.1 also shows a constant level between 0.2 and 0.3 ns^{-1} across the whole wafer.

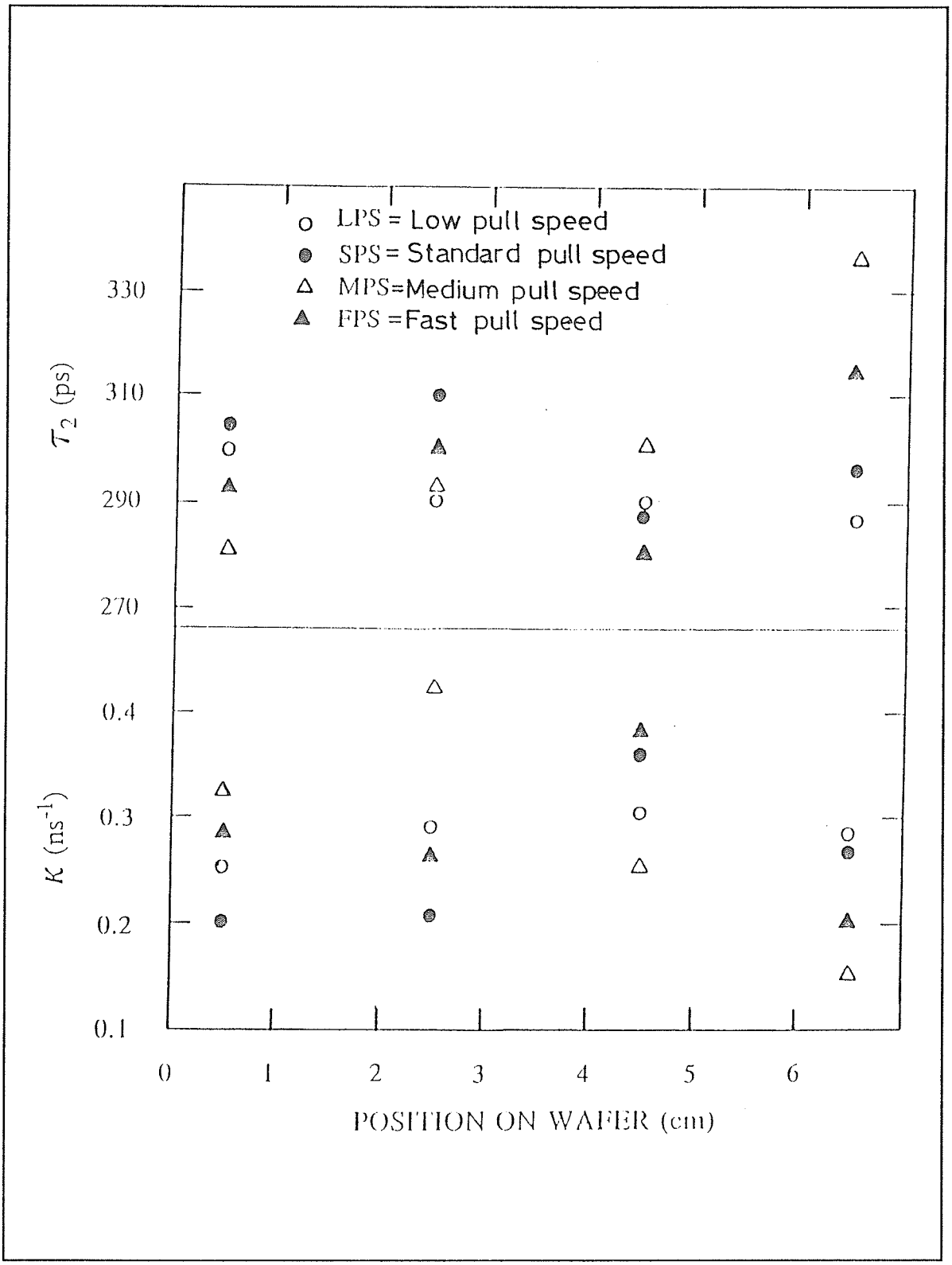

Figure 6.1 Main lifetime component, τ_2 and the trapping rate κ as a function of measurement position across the wafers.

6.2.3 Discussion

There are several interesting observations to be made. One is that both monovacancies and divacancies are present since the vacancy related lifetime τ_2 has values which are in between the monovacancy and the divacancy values. Second, there seems to be no obvious changes in the lifetime characteristics as one moves from the edge of the wafer towards the centre. This is in contrast to the early study (132) on different wafers which showed significant change in the defect concentration and distribution across a given wafer. It seems that the present wafer material is more homogenous despite the fact that the wafers are six inches in diameter as compared to four-inch wafers investigated in (132).

The third and final observation is that there seem to be no influence of the pull speed on the concentration of vacancy-type defects and their distribution across the wafers.

6.2.4 Conclusion

The positron data have shown that no obvious systematic variation in the defect configuration over the cross section of a given wafer. The data also show a homogenous distribution of vacancy-related defects across the wafer in contrast to what has been found in Ref. (132). Finally, the pull speeds during the growth of the ingots have no apparent influence on the defect characteristic across the six-inch Cz-silicon wafers.

6.3. HEAT TREATMENT INDUCED DEFECTS IN CZ-SILICON

This section deals simply with the investigation of vacancy-type defects induced by heat treatments such as RTA and furnace annealing in the Cz-silicon material. The samples used in this investigations were B-doped material and heavily Sb-doped material. The focus of the investigation is directed towards examining the type of defects observed in the material, the role of the dopant in trapping of vacancies and the temperature dependent configurations of the complexes.

6.3.1. Samples

Four sets of samples were investigated. Set I was boron doped (~10 Ωcm) and contained ~$1.5\times10^{18}/cm^3$ oxygen interstitials and less than ~$1\times10^{15}/cm^3$ substitutional carbon. This set was subjected to rapid thermal annealing (RTA) between 600 and 1000°C. A different wafer was used for each RTA temperature. Set II samples (of the same type as in Set I) were subjected first to a particular pre-heat-treatment (denoted CES-6), as shown in Figure 6.2. This reduced the (average) oxygen interstitial concentration to $1.8\times10^{17}/cm^3$, but subsequent RTA annealing between 700 and 800C increased the (average) concentration to $1\times10^{18}/cm^3$. Set III samples were heavily doped with Sb (0.01-0.02 Ωcm) and heat-treated by RTA only, while set IV samples received the same pre-heat treatment as for the set II samples.

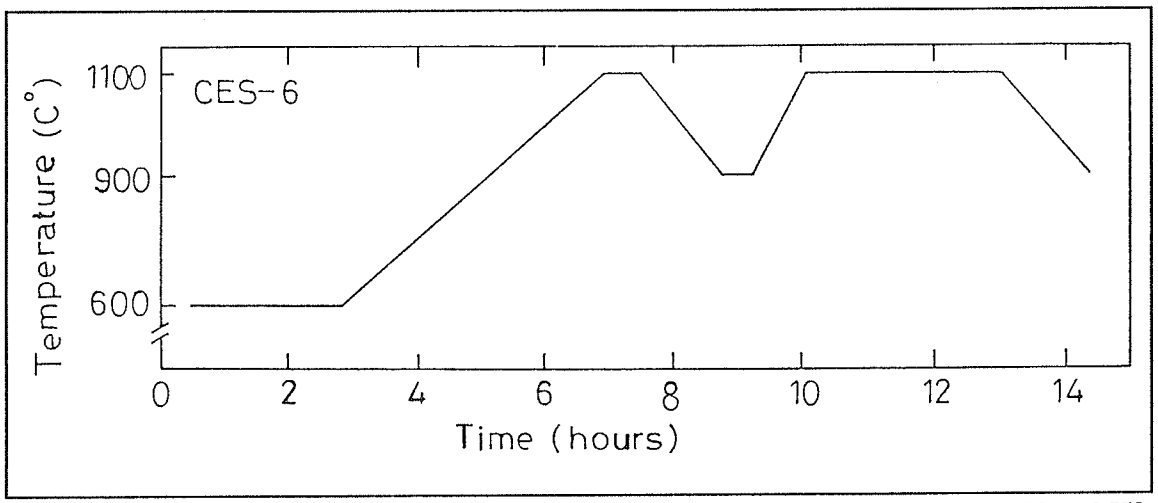

Figure 6.2 Scheme for the CES-6 pre-heat-treatment employed for sample sets II and IV.

6.3.2. Results

Figure 6.3 displays the defect lifetime τ_2 for set I and II samples, and the trapping rates. A trapping rate of $1ns^{-1}$ corresponds to a vacancy concentration of 1x1017 $/cm^3$. The fact that the values for τ_2 are larger than the bulk lifetime [218 ps in silicon (133)] shows that the defects detected are of vacancy-type. In the case of the set I samples (filled circles in Figure 6.3) the

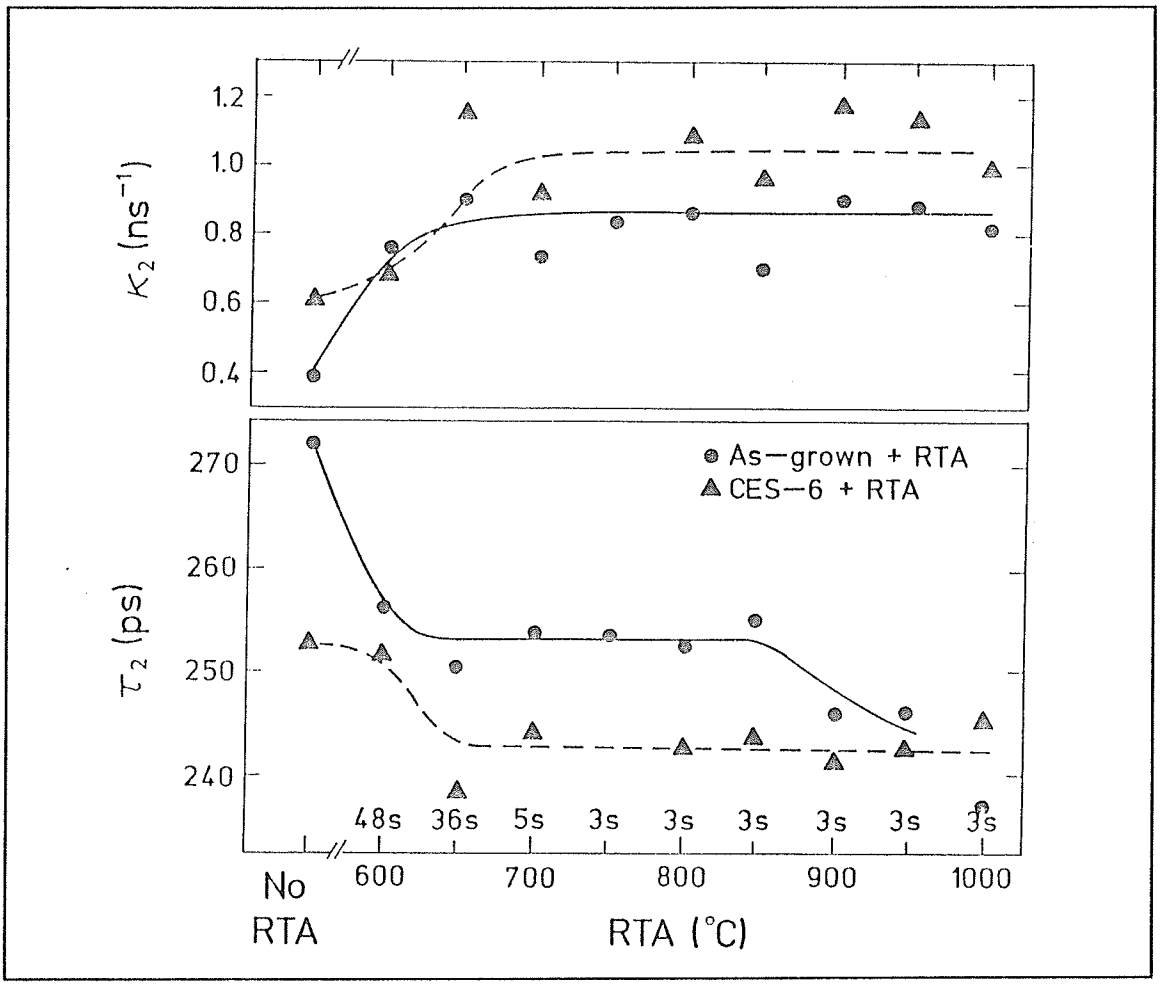

Figure 6.3 Trapping rates κ_2 and defect lifetime τ_2 for as-grown RTA treated and CES-6 pre-treated boron doped Cz-Si. The times indicate RTA duration.

effect of RTA is initially to decrease the value of τ_2 from 270 to $\approx$250ps and later on ($\approx$900 C) to 240ps. The lifetime of 270ps in the as-grown samples arises from monovacancies (133). The trapping rate increases rather abruptly upon RTA between 600 and 700 C but stays constant between 650 and 1100C at a level 2 times higher than for the as-grown material.

For set II, the pre-heat-treatment itself results in a lower positron lifetime of 250ps and the amount of vacancies is increased slightly compared to the untreated case. The RTA treatment further reduces the positron lifetime (to 240ps), but results in a similar behaviour of the trapping rate as found for the set I samples.

Since changes in trapping rate as well as in lifetimes can be effected by changes in the charge

state of the defects (134), low temperature measurements were also conducted. In particular, net negatively charged vacancy complexes would show a strongly increased trapping rate at low temperatures. In Figure 6.4, we have the results for 3 different samples, 2 from Set I and 1 from Set II. Between 30 and 300 K the 3 samples exhibit only a weak temperature dependence (τ_2 increases with temperature), which rules out the presence of negatively charged defect complexes.

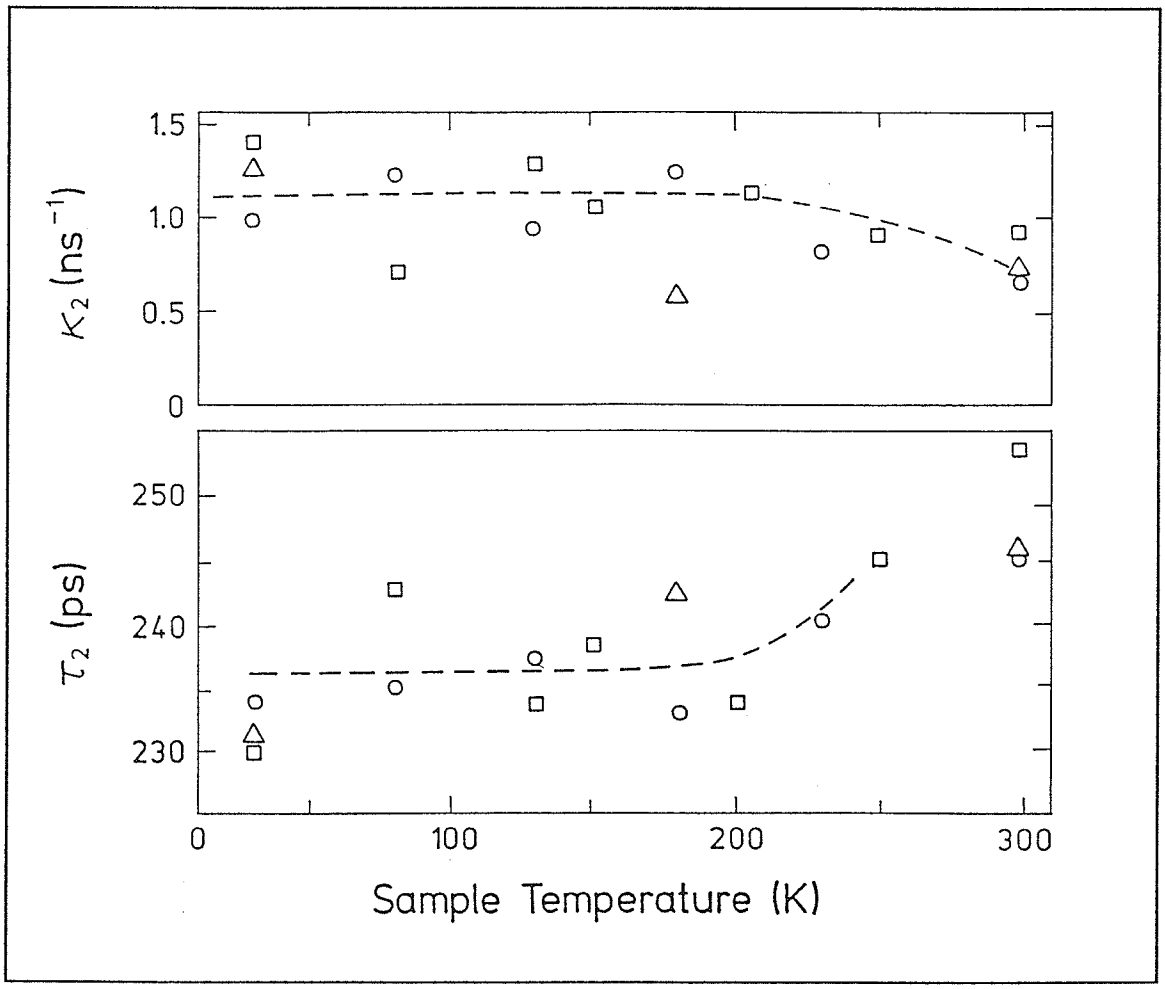

Figure 6.4: Low temperature results for 3 boron doped samples subjected to heat-treatments as indicated by □ RTA at 850°C. ○ RTA at 900°C. △ RTA at 900°C plus CES-6 pre-treatment.

The heavily Sb-doped samples were only investigated at room temperature. As shown in Figure

6.5, the heavy Sb doping does not change the value of the defect lifetime, and increases only slightly the trapping rate. RTA, either on as-grown or on CES-6 pre-treated samples, results in a behaviour much different from that shown in Figure 6.3.

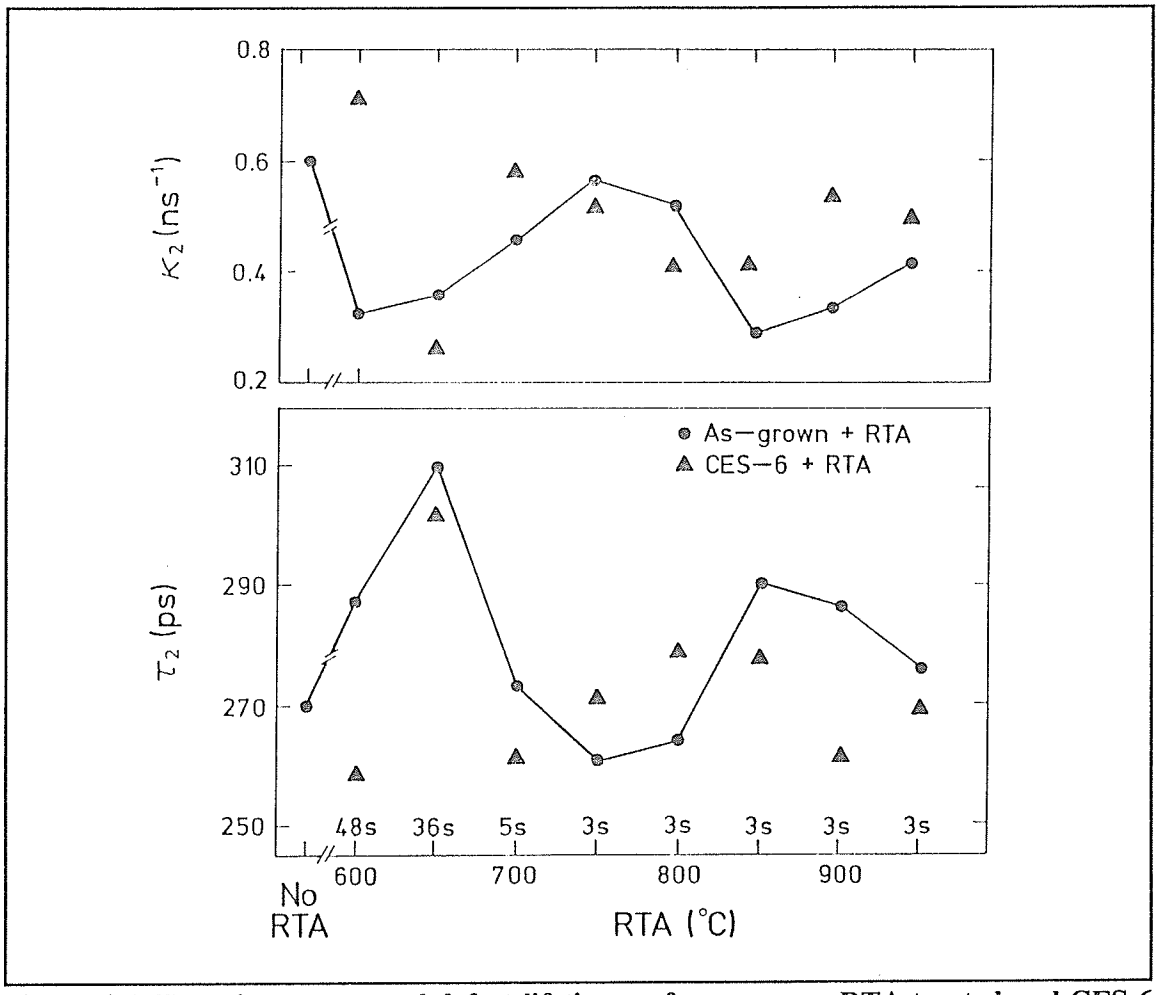

Figure 6.5: Trapping rate κ_2 and defect lifetime τ_2 for as-grown RTA treated and CES-6 pre-treated Sb-doped Cz-Silicon. Curves shown are only intended as a guide to the eye.

6.3.3 DISCUSSION

For both the B-doped and the Sb doped samples, the value of τ_2 indicates that in as-grown Cz-Si the vacancies, which must be bound to some trap, are unperturbed in the sense that their open volume corresponds to that for free monovacancies. The amount of trapped vacancies is 0.4 (B-doped) and 0.6 (Sb-doped) x 10^{17}/cm^{-3} using the calibration for neutral defects as found by

Mascher *et al* (134). Vacancy-traps in this concentration range would likely be oxygen clusters (in the B-doped material) as suggested earlier (135,136). This means that a considerable fraction of all available oxygen is in a clustered form.

The observation that RTA has an effect on the as-grown samples at all is somewhat surprising in view of the fact that during the cool-down of the original ingot the samples spend a considerably longer time at any temperature than they did later on during the RTA. To explain our observations on the B-doped samples we suggest that due to the fast cool-down of the RTA treated wafers, high-temperature configurations of the grown-in vacancy-impurity complexes can be quenched in. These are missing in the slowly cooled wafers thus accounting for the increase in trapping rate with RTA (see Figure 6.3). RTA does not appear to create additional complexes beyond those which are grown-in since the trapping rate is constant above 650 C.

The high-temperature configurations corresponds to a "squeezed" vacancy-impurity complex because the τ_2 lifetime decreases from the 270ps level. From Figure 6.3 we note that CES-6 furnace annealing of the wafers also decreases the value of τ_2 and increases the trapping rate. In view of the above, this can also be explained by the faster cooling rate from 900 C of the wafers than for the original ingot, albeit not as fast as for the subsequent RTA treatments.

The RTA of the CES-6 pretreated samples indicate that the quenched-in vacancy-impurity complex is made observable already at 650 C and is independent of temperature up to 1000 C. The characteristic lifetime is close to 240ps. For the as-grown samples this lifetime is first found after 900 C of RTA which indicates that the defects responsible for the 270ps lifetime transform into the 240ps species. The constant level of 250ps between 650 and 850 C is simply the weighted average of the 270ps and the 240ps lifetimes. We note that this indication for the thermal instability of these defects is supported by the observation that the 270ps lifetime was not prominent after the CES-6 treatment which had a "fast" cool-down from 900 C. We finally note

that the constant level of the trapping rates for the CES-6 treated samples is 25 % higher than for the as-grown materials. This may well be related to a higher oxygen cluster concentration as suggested by the significant decrease in the average interstitial concentration.

The low temperature measurements suggest that further complexes can be detected at low temperatures in which the vacancies are even further "squeezed". These are not observed at higher temperatures probably because they are shallow traps.

For the Sb-doped samples, it is evident from Figure 6.5 that Sb significantly modifies the annealing behaviour. In particular, annealing at 650 C indicates formation of divacancies (5), and, generally, vacancy responses are above 260ps. Sb at high concentrations appears to dominate as a vacancy trap.

6.3.4 CONCLUSION

The present positron lifetime investigations show that vacancies are retained in Cz-grown Si. The vacancies are probably trapped by oxygen interstitial clusters during the cool-down of the ingot. In slowly cooled samples, a lifetime of 270ps indicates unperturbed monovacancies. In rapidly cooled samples, RTA indicates that perturbed ("squeezed") vacancies exist between 650 and 1000 C, and that the unperturbed vacancies transform to the perturbed ones around 900 C. In heavily Sb-doped samples, Sb appears to dominate as a vacancy trap.

6.4 THE EFFECTS OF OXYGEN INTERSTITIALS AND CARBON IMPURITIES ON THE THERMAL DONOR KINETICS

Oxygen and carbon are the two most common impurities unintentionally introduced during the crystal growth of silicon by various methods. Their behaviour has extensively been investigated for several decades (137,138) because of their potential influence on the quality of various silicon

electronic devices. When distributed homogeneously in the crystalline bulk as point-type defects, they are electrically inactive and harmless. However, during high temperature processing steps, they may migrate, interact, and pair with other defects forming new electrically active complexes or promoting different precipitating processes.

Most of the studies have been done on Cz-grown silicon crystals (139) with supersaturated oxygen concentration in excess over the carbon concentration. It has been indicated previously (140,141) that the ratio of oxygen-carbon concentration may influence significantly the precipitation processes at high temperatures; that is, the high carbon silicon may behave differently. Therefore, in this study we present new results on defect interactions and the effects of carbon impurities and oxygen interstitials on the thermal donor kinetics.

6.4.1 Samples

The specimens used in these experiments were cut from a p-type boron doped Cz-silicon wafers. The concentrations of interstitial oxygen and substitutional carbon atoms were determined by Fourier transformation infrared (FTIR) with the results prescribed in Table I. The samples had

TABLE I. The characteristics of specimens.

Crystal	Res. (Ω cm)	$[O_i]$ Con.(cm^{-3})	$[C_s]$ Con.(cm^{-3})	Cond. type
A	~ 7	1.5×10^{18}	7.5×10^{16}	p
B	10	$\sim 10^{18}$	$< 10^{15}$	p

first undergone 450°C furnace annealing for a time duration of 64 hours, in order for the thermal donors to be generated. After only one hour of furnace annealing treatment, the material changed the conductivity type from a p-type to n-type. The resistivity of crystal A was 0.9 ohm-cm after

receiving 64h of annealing. In the case of crystal A, some samples were investigated during the thermal donor generation. After the 64h of annealing, the samples were treated by rapid thermal heat treatment for 2, 5, and 10 seconds for various temperatures ranging from 650 to 800°C, while 2 and 5 seconds were employed at temperatures between 850 - 1000°C.

The thermal donor annihilation kinetics studies showed that the sample which was treated for 2 seconds of rapid thermal heat treatment changed the conductivity type from n-type back to the original p-type between 725 and 750°C at which point the resistivity was about 55 Ω-cm.

Heat treatments at lower temperatures were done at our laboratory where the samples were placed inside a horizontal Al_2O_3 tube so that the samples rested along two edges only. Sample B, after 64h/450 C annealing has been subjected to RTA treatment at 725 C for 2, 5, and 10 seconds. All lifetime measurements in this section were conducted at room temperature.

6.4.2 Results

All the points plotted in the figures are an average of 3-5 measurements. In Figure 6.6 is shown on the top panel the variation of the total concentration of thermal donors generated at 450 C versus heat treatment duration. The thermal donor concentration increased rapidly from 0.2×10^{15} cm^{-3} to a level of 5.1×10^{15} cm^{-3} in a period of annealing time between 0.5h to 32h, after which it started to level off towards a saturation level of 5.5×10^{15} cm^{-3} for the rest of the annealing duration up to 64h. Also in Figure 6.6 are shown the defect lifetime τ_2 (middle panel) and the trapping rate κ (lower panel) as a function of annealing time. We observe from the defect lifetime panel that there is no change in the defect lifetime up to 32h of annealing and the value for τ_2 is $\sim$ 276ps. The defect lifetime then began to increase reaching a value of τ_2 = 307ps as the annealing time increased from 32h to 64h. The trapping rate in the lower panel has a constant value = 0.34 ns^{-1} between 0.5h and 32h of annealing and then decreased to about 0.2 ns^{-1} after 64h of annealing.

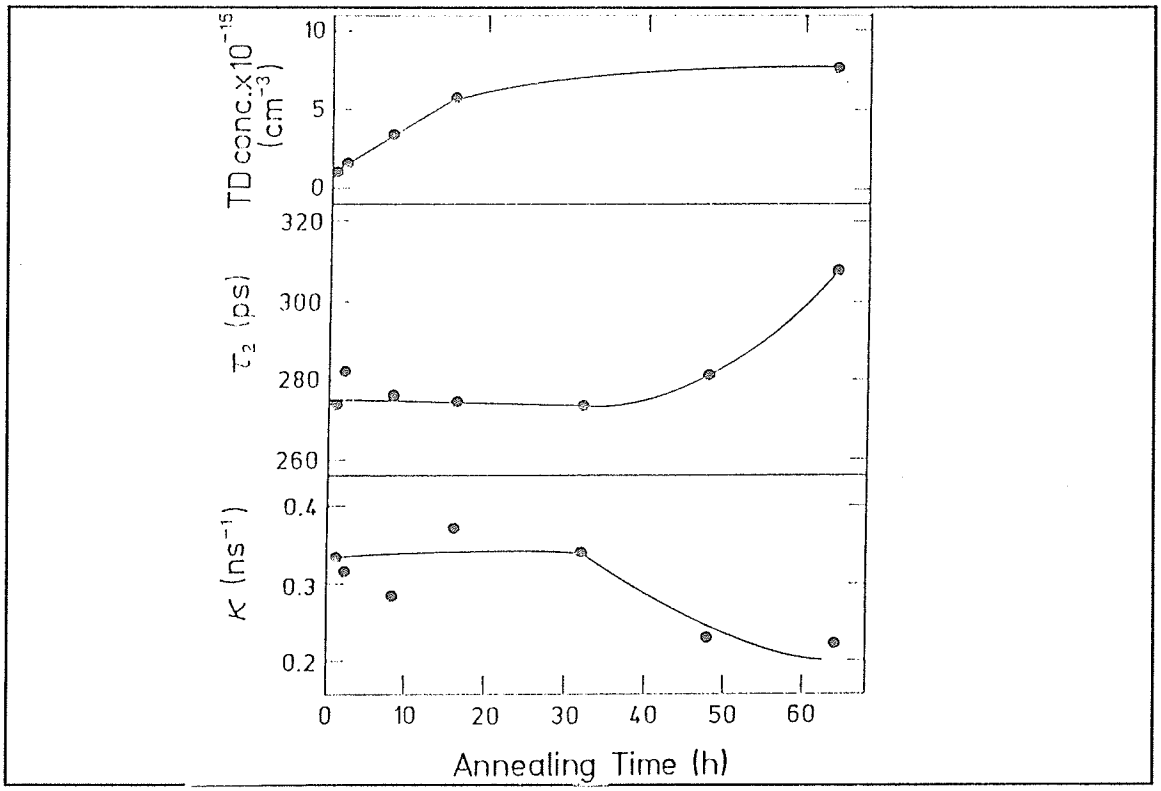

Figure 6.6. Crystal A has undergone pre-heat treatment at 450C for the thermal donor generation.

The collection of results plotted in Figure 6.7 represents rapid thermal annealing of samples in the temperature range of 650 - 1000C. We observe that annealing at 650C results in no change in the defect lifetime τ_2 (310ps) and that the trapping rate was constat at a value of $\kappa = 0.2ns^{-1}$. The thermal donor concentration is constant after 2s of RTA annealing at a value of $5x10^{15}$ cm^{-3}. At 700C, the results showed slight indication for a decrease in the trapping rate but the lifetime remained constant at the same level as before. During this annealing all the thermal donors have been removed.

At 725C the defect lifetime decreases towards 270ps and this decrease is realized also at 750C , albeit at a faster rate. Between 775C and 900C, the lifetime tends to increase after the initial decrease. Finally, at 1000C the lifetime steadily decreases, reaching a low value of 260ps. The trapping rate increases during the decrease in the lifetime values and decreases during the

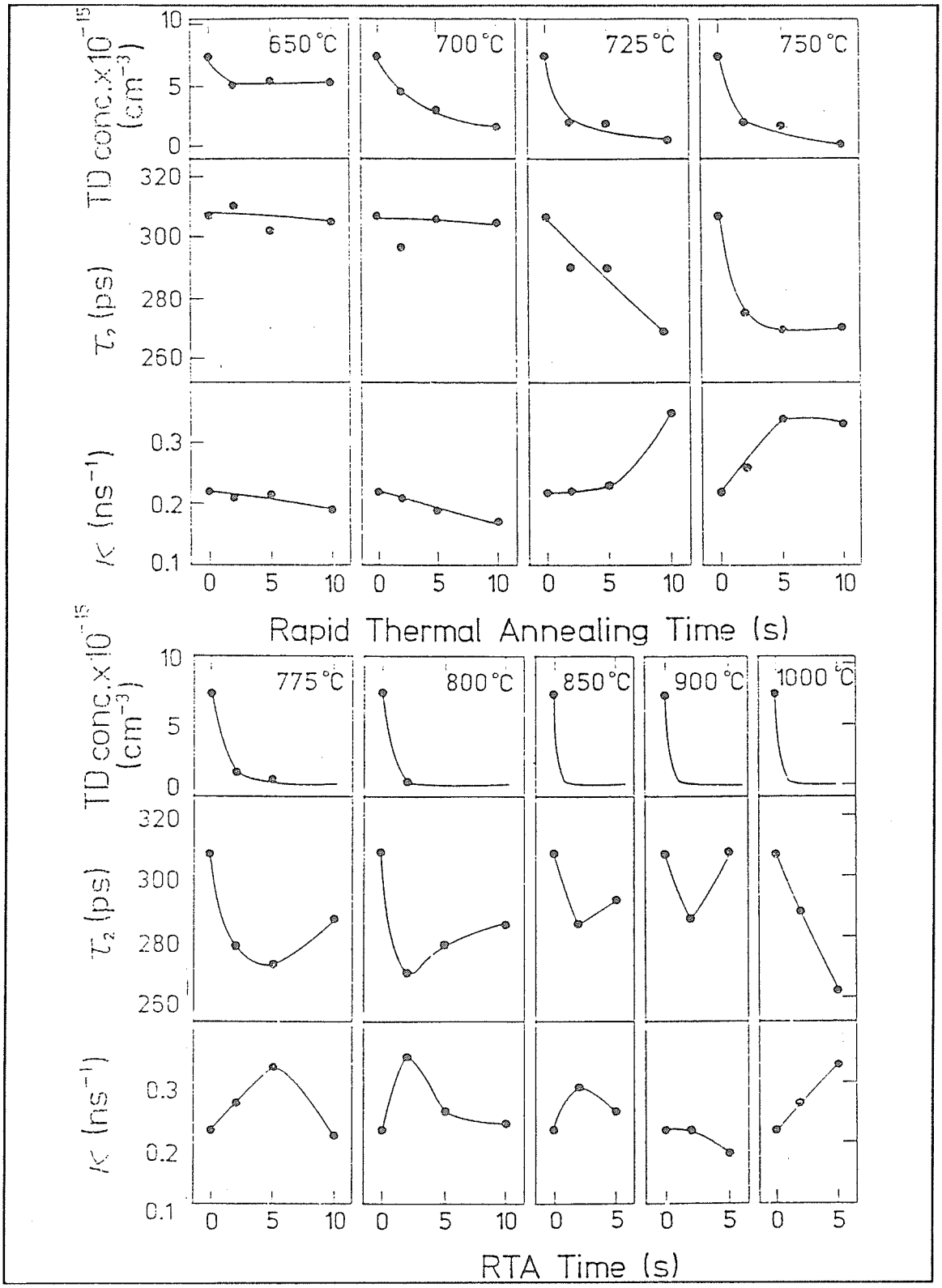

Figure 6.7. Rapid Thermal Annealing for crystal A at various temperatures between 650C and 1000C.

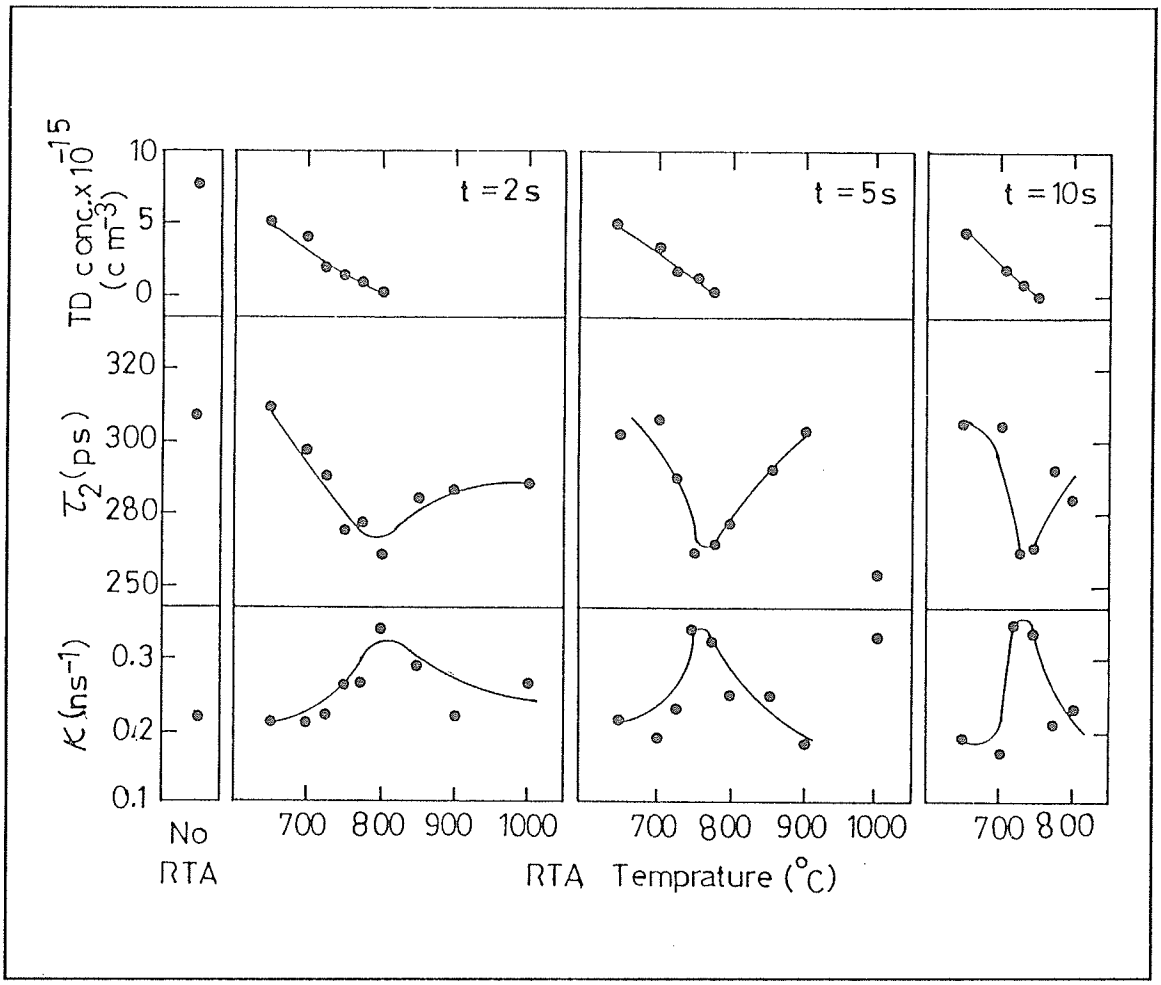

Figure 6.8 Represents the collection of results obtained in Fig. 6.7 plotted as function of RTA temperature.

subsequent increase in lifetimes with temperatures at or above 775C.

The data shown in Figure 6.7 are represented in Figure 6.8 which displays the development with temperature for a fixed time (2s, 5s or 10s) of RTA at each temperature. This figure indicates clearly that the vacancies present initially in the samples are transformed to monovacancies, as indicated by the lifetime value of 270ps, between 725C (10s RTA) and 800C (2s RTA) and that subsequent higher annealing temperatures result in an increased contribution from vacancy agglomerations.

Figure 6.9 shows isothermal annealing experiments at 725 C for the samples containing zero crbon concentration. The results of the figure show that as TD concentration decreases from

$2x10^{16}$ cm^{-3} to $0.3x10^{16}$ cm^{-3}, the defect lifetime increased slightly from 284ps to 301ps while the trapping rate decreases from 0.32 to 0.22 ns^{-1}. We note that the thermal donor concentrations is higher in this than sample in the carbon containing samples (Figure 6.7,6.8). We further note that the time developments of τ_2 and κ do not correspond to that displayed (at 725°C) in Figure 6.7.

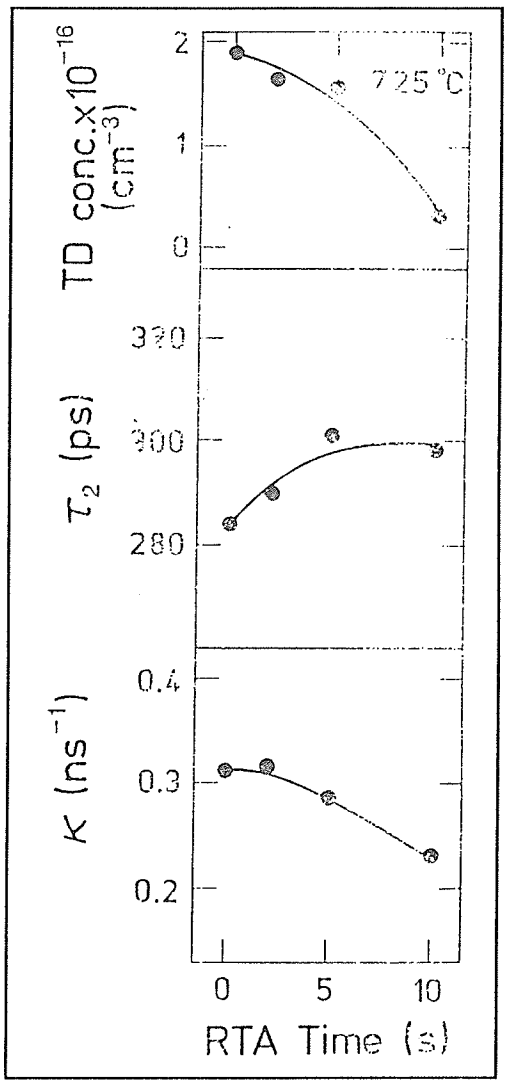

Figure 6.9 RTA treatments at 725C for samples containing no carbon impurities.

6.4.3 Discussion

The interpretation that can be drawn from the results shown in Fig. 6.6 is that the concentration of thermal donors rapidly increases during the first 16 hours of heat treatment and slowly approaches a level of saturation of $5.5x10^{15}$ cm^{-3} after 20 hours of annealing. During the formation of the thermal donors no changes are occurring in the lifetime parameters until after 32 hours of annealing. It is not surprising that thermal donors are ineffective positron traps since they are positively charged.

Since the bulk lifetime was constant (214 with uncertainty of 5ps in good agreement with the established bulk lifetime of 218 ps) throughout the heat treatments this indicates that oxygen clusters, as found by Dannefaer et al (142), are not found in detectable amounts.

During the first 32 hours of annealing, the vacancy related lifetime τ_2 was constant at 278 ps. This lifetime is between that for monovacancies 270 ps, (143) and that for the divacancies 325ps

(143), showing that both types of vacancies contribute to the observed lifetime. The balance between the amount of these vacancies remain constant up to approximately 32 hours of annealing.

The argument that can be made for not seeing any changes during 32 hours of annealing is that the average migration distance for the oxygen interstitials and the distance between two nearest vacancies are somewhat large in order for them to get trapped by the vacancy traps. The average migration distance can be calculated according to the following:

$$<l> = \sqrt{Dt} \tag{1}$$

Where t is the annealing time and D is the diffusitivity of interstitial oxygen and has found to be (144) ;

$$D = 0.17\exp(-2.54/kT) \quad \text{cm}^2/\text{s} \tag{2}$$

Substituting for $t = 1.1\text{x}10^5$ s (32 hrs.) and T=723 K, the diffusitivity D is equal to $3.29\text{x}10^{-19}$ cm^2/s. The average migration distance as calculated using Eq. (1) is found to be $\sim$19Å where in reality it is ten times higher than the calculated value. The calculations of the distance between two vacancies is given below as an illustration as to why there was no detectable variation during the 32h of annealing at 450C. The τ_2 lifetime is a weighted average of the mono-and divacancy lifetimes:

$$\tau_2 = \frac{(I_v\tau_v + I_d\tau_d)}{(I_v + I_d)} \tag{3}$$

$$I_2 = I_v + I_d \tag{4}$$

where τ_2 is the defect lifetime obtained from figure. 6.6, τ_v is the monovacancy lifetime, τ_d is the divacancy lifetime, I_v is the intensity for the monovacancy and I_d is the intensity for the divacancy and I_2 is the intensity of the defect.

Using the trapping model which was discussed earlier in section 2.6.2 we will be able to calculate the concentration of these defects. The trapping rate for two deep traps will be as follows:

$$K_d = \frac{I_d}{I_1}\left[\frac{1}{\tau_B} - \frac{1}{\tau_v} + \frac{I_v}{\tau_d} - \frac{I_v}{\tau_v}\right] \tag{5}$$

$$K_v = \frac{I_v}{I_1}\left[\frac{1}{\tau_B} - \frac{1}{\tau_v} + \frac{I_d}{\tau_v} - \frac{I_d}{\tau_d}\right] \tag{6}$$

where τ_B is the bulk lifetime and I_1 is the intensity for the short lived lifetime component. Evaluating the values of all the parameters at t= 32 hours of annealing, it has been found that the divacancy concentration is equal to $\sim 3\times10^{15}$ cm-3 and the mono vacancy concentration is equal to $\sim 2\times10^{16}$ cm^{-3}. So in order to determine the distance between two vacancies we obtained the number of silicon atoms per vacancy to be equal to $\sim 2\times10^{7}$. Thus the average distance between two vacancies is determined by $<l_d> = (N_d)^{1/3}$ x (distance between two nearest atoms), where N_d is the number of Si atoms per divacancy and the value was found to be 500Å. As we have mentioned above, the actual migration distance is ten times higher than the calculated value (19Å). This result explains to a certain extent the reason for not seeing any variations during 32h of annealing.

The result of Figures 6.7 and 6.8 are a collection of RTA measurements at various temperatures between 650C and 1000C. As the thermal donors get annealed out at 650C (where in fact they

change configurationally), we notice no change in the lifetime as well as in the trapping rate which agrees with the absence of an effect when they are created. As temperature increases to 725C, the defect lifetime decreases from 308ps to a monovacancy level of $\sim$ 270ps and the trapping rate increases from $\sim$ $0.2ns^{-1}$ to $0.35ns^{-1}$. When we get to a higher temperature 775C, the monovacancies become unstable and very mobile. Meanwhile, the oxygen interstitials tend to form larger and more stable clusters, so we see an increase in the defect lifetime to the original value of 308 ps (close to the divacancy level of 325 ps), and the trapping rate declines to the original value as well.

At 1000C, the lifetime decreases to a low value of 260ps and the trapping rate increases to a value of $0.35ns^{-1}$. The data obtained in section 6.2 for the RTA heat treatment induced defect showed that the high temperature configurations (>900C) correspond to a "squeezed" vacancy-impurity complex with a lifetime of 240 ps. In comparison to the results obtained in this section at 1000C, it is suggested that such "squeezed" vacancies are formed.

Figure 6.9 shows the results obtained for the samples containing no carbon concentration. Several observations can be made; One is that the results indicate a slight increase in the trapping rate compared to the 1.5 ppm carbon doped sample at the same temperature. A second observation is that there a relatively more monovacancies than divacancies compared to the carbon doped samples. The third observation is that the thermal donor concentration is also higher in the non carbon doped sample than in the carbon doped ones and this can be expected since carbon can suppress the thermal donor formation.

6.4.4. Conclusion

The results show that during thermal donor generation at 450C, the monovacancy response decreases relative to the divacancy response after 32h of annealing time. The RTA of the thermal

donors indicates a process which begins to take place at 725C during which the divacancies are converted into a monovacancies. No correlation was evident between thermal donor concentration and vacancy response. The results of the samples without carbon differed significantly from the samples with carbon. Further research is necessary in order to have a better understanding of the behaviour of carbon in these samples.

REFERENCES

1) Eldrup, M.,"Positron Lifetimes in Water and Ice, and in frozen Aqueous Solutions\1" Ph.D. Thesis (1971). Danish Atomic Energy Comission Research Establishment Ris\7f 1Chemistry Department, Lyngby,Denmark. p7.

2) Dirac, P.A.M., A Theory of Electrons and Protons. Proc. Roy. Soc. A126, 1360-36 (1930).

3) Anderson, C.D., The Apparent Existance of Easily Deflectable Positives. Science, New Series 76, 238-239 (1932).,C.D. Anderson, The Positive Electron, Phys. Rev. 43, 491-494 (1933).

4) Blackett, P.M.S., and G.P.S. Occhialini, Some Photographs of the Tracks of Penetrating Radiation. Proc. Roy. Soc. A139, 699-726 (1933).

5) Tribaud, J., Phys. Rev. 46, 781 (1934).

6) Klempere, O., Proc. Cambridge Phil. Soc. 30, 347 (1934).

7) Hanson, N.R., The Concept of the Positron. Cambridge University Press p236 1963).

8) DeBenedetti, S., C.E. Cowan and W.R. Konneker, Phys. Rev. 76, 440 (1949).

9) Ashcroft, N.W., and \ N.D. Mermin, Solid State Physics. Cornell University, Saunders Company, Phil. U.S.A. p616 (1976).

10) Cotterill, R., The Cambridge Guide to the Material World.The Technical University of Denmark, Cambridge University Press p69 (1985).

11) Kittel, C., Introduction to Solid State Physics. sixth edition, p73 (1986).

12) K. Seeger, Semiconductor Physics.Springer Series in Solid-State Sciences p1 (1982).

13) Corbett, J., Electron Radiation Damage in Semiconductors and Metals. Academic Press Inc. p1 (1966).

14) Ashcroft, N.W., and N.D. Mermin, Solid State Physics. Cornell University, Saunders

Company, Phil. U.S.A. p564, 577 (1976).

15) Simpson, R.E., Introductory Electronics for Scientists and Engineers. Second Eidition, University of New Hampshie, Allyn and Bacon Inc. p168 (1987).

16) Lannoo, M., and J. Bourgoin Point Defects in Semiconductors I. Theoretical Aspects, Springer Series in Solid State Sciences 22 p232 (1981).

17) Goldanskii, V.I., Physical Chemistry of the positron and Positronium. Atomic Energy Review 6, p1-148 (1968).

18) Hautojarvi, P., Positrons in Solids, Topics in Current Physics **12**, p2 Berlin-Heidelberg-New York, Springer-Verlag, (1979).

19) Hautojarvi, P., Positrons in Solids, Topics in Current Physics **12**, p3 Berlin-Heidelberg-New York, Springer-Verlag, (1979).

20) Brandt, W., and A. Dupasquier, Positron Solid State Physics. Proc. of theinternational School of Physics "Enrico Fermi." Course LXXXIII. North Holland p566 (1983).

21) Schultz, P.J., and K.G. Lynn Rev. Mod. Physics 60 p701 (1988).

22) Wilsey, N.D., J.R. Karins, J.B. Shapiro, Vijay A. Singh and J.W. Corbett, Inst. of Physics Conf. Ser. **59**, Chap. 2 (1981).

23) Puska, M.J., O. Jepsen, O. Gunnarson, R.M. Nieminen, Phys. Rev. B**34**, 2695 (1986).

24) Hautojarvi, P., Positrons in Solids, Topics in Current Physics 12 Berlin-Heidelberg-New York, Springer-Verlag, (1979).

25) Brandt, W., and A. Dupasquier, Positron Solid State Physics. Proc. of the international School of Physics "Enrico Fermi." Course LXXXIII. North Holland (1983).

26) Krause, R., G. Dlubek and O. Brummer, Positron Studies of Decomposition Phenomena in Al Alloys. Proceeding of the European Meeting on Positron Studies of Defects, Germany (1987).

27) Dannefaer, S., P. Macher and D. Kerr, J. Appl. Physics Condensed Matter p3213 (1989).

28) Dannefaer, S., and D. Kerr, Oxygen in Silicon: A positron annihilation investigation. J. Appl. Physics 60 (4) (1986).

29) De Vries, J.,A. Zeoca, R.S. Brusa, R.G. Grisenti, S. Oss, and A.van Veen. in: Positron Annihilation. Ed. L. Dorikens-Vanpraet, M.Dorikens and D. Segers. (World Scientific) p654 (1989).

30) Moszynski, M., Nucl. Instr. and Meth. 134 p77 (1976).

31) Kirkegard, P., N.J. Pedersen and M. Eldrup: PATFIT-88, Riso-M-2740 (1989), Riso, DK-4000 Roskilde Denmark.

32) Kittel, C., Introduction to Solid State Physics. sixth edition, p208,209 (1986).

33) Curtis, O.L., "Effects of point defects on electerical and optical properties of semiconductlrs", Point Defects in Solids v2, J.H., Crawford, L.M. Slifkin Edts, Plenum Press, New York (1975) p260.

34) Nichols, C.S., C.G. Van de Walle, and S. T. Pantelides, Phys. Rev. Lett. **62**, 1049 (1989).

35) Gourary, R.S., and A.E. Fein, J. Appl. Phys. **33**, 331 (1962).

36) Friedel, in *Radiation Effects on Semiconductors Components*, Ed. by F. Cambeu vol.1 (1967).

37) Messmer, R.P., and G.D. Watkins, Phys. Rev. Lett. **25**, 656 (1970).

38) Bennemann, K.H., Phys. Rev. **137**, A1497 (1965).

39) Callaway, J., and A.J. Hughes, in *Radiation Effects in Semiconductors*, Ed. by F.L. Vock (Plenum Press, New York, 1968) p27.

40) Seeger, A., and A. Scholz, Phys. State Sol. **3**, 1480 (1963).

41) Watkins, G.D., in: Radiation Damge and Defects in Semiconductor. Inst. Phys. London, (1973) p228.

42) Watkins, G.D., in: *Radiation Effects in Semiconductors*, Ed. by F. Cambeu vol.1 (1967).

43) Watkins, G.D., Trans. IEEE N5-16 (6), 13 (1969).

44) Watkins, G.D., and J.W. Corbett, Phys. Rev. **138,** A543 (1965).

45) Brower, K.L., Rad. Eff. **8,** 213 (1971).

46) Lee, Y.H., and J.W. Corbrett, Phys. Rev. B**8,** 2810 (1973).

47) Watkins, G.D., Phys. Rev. **155,** 802 (1967).

48) Watkins, G.D., and J.W. Corbett, Phys. Rev. **121,** 1001 (1961).

49) Bean, A.R., R.C. Newman, and R.S. Smith, J. Phys. Chem. Solids, **31,** 1300 (1959).

50) Brelot, A., in: *Radiation Damage and Defects in Semiconductor*, (Inst. of Phys., London, 1973) p 191.

51) Bean, A.R., R.C. Newman, and R.S. Smith, J. Phys. Chem. Solids, **31,** 1300 (1959).

52) Bean, A.R., and R.C. Newman, Sol. State Comm. **8,** 175 (1970).

53) Newman, R.C., and R.S. Smith, J. Phys. Chem. Solids **30,** 1493 (1969).

54) Brown, W.L., and W.M. Augustymak, J. Appl. Phys. **30,** 1300 (1959).

55) Benki, G., and C.A. Dins, J. Appl. Phys., **35,** 293 (1964).

56) Cheng, L.J., C.K. Yeh, S.I. Ma, and C.S. Su, Phy. Rev. B**8,** 2880 (1973).

57) Cheng, L.J., C.K. Yeh, Solid St. Commun. **12,** 529 (1973).

58) Brandt, W., and L.J. Cheng, Phys. Lett. A**50,** 475 (1977).

59) Sen, P., and C. Sen, J. Phys. C**7,** 2776 (1974).

60) Dorikens, M., C. Dauwve, and L. Dorikens-Vanpret, Appl. Phys. **4,** 271 (1974).

61) Dannefaer, S., G.W. Dean, D.P. Kerr, and B.G. Hogg, Phys. Rev. **B14,** 2709 (1976).

62) Fubs, U. Holzhauer, S. Mantl, F.W. Richter, and R. Sturm, Phys. Stat. Sol. (b) **89,** 69 (1978).

63) Dannefaer, S., G.W. Dean, D.P. Kerr, and B.G. Hogg Phys. Rev. **B14,** 2709 (1976).

64) Kelly, J.J., and R.M. Lambrecht, Phys. Lett. **60A,** 475 (1977).

65) Kasier, W., H.L. Frisch, and H. Reiss, Phys. Rev. **112**,1546 (1958).

66) Lax, M., Phys. Rev. **119**, 1502 (1960).

67) Stein, H.J., in: Radiation Effects in Semiconductors, J.W. Corbett and G.D. Watkins (Eds.) Gordon and Breach, 1971).

68) Hirata, M., H. Saito, and J.H. Crawford Jr. in: lattice Deffects in Semiconductors, R.R. Hasiguti (Eds.) Univ. of Tokyo Press, 1968).

69) Watkins, G.D., Phys. Rev. **B13**, 2511 (1976).

70) Young-Hoon Lee, and J.W. Corbett, Phys. Rev. **B13**, 2653 (1976).

71) Fuller, C.S., H.A. Ditzenberger, N.B. Hanny and Buehler, Phys. Rev. **96**, 833 (1954).

72) Wagner, P., Infarared Absorbtion studies of thermal donors in silicon. NMR v59 p125 1986

73) Spenth, M,. MRS Symp. Proc. 1986, vol. 59, p.111.

74) Kimerling, L.C., MRS Symp. Proc. 1986, vol. 59, p.83.

75) Snyder, L.C., MRS Symp. Proc. 1986, vol. 59, p.207.

76) Borenstein, J., J.W. Corbett, MRS Symp. Proc. 1986, vol. 59, p.173.

77) Oates, A.S., R.C. Newman, J.M. Tucker, G. Davies and E.C. Lightowlers, MRS v59

78) Newman, R.C., J. Phys. C: Solid State Phys. **18**, L967, (1985).

79) Tan, T.Y., MRS Symp. Proc. 1986, vol. 59, p.195.

80) Tan, T.Y., MRS Symp. Proc. 1986, vol. 59, p.269.

81) Newman, R.C., J. Phys. C: Solid State Phys. **18**, L967, (1985).

82) Newman, R.C., MRS Symp. Proc. 1986, vol. 59, p.403.

83) Newman, R.C., J. Wakefield, Proc. Int. Conf. on Solid State Phys. in Electron and Telecom. Brussels 1958 p318-28 Ed. by M. Desirant and J.L. Michiwls (Acadamic Press: New York)(1960).

84) Hall, R.N., J. Appl. Phys. 29, 914 (1958).

85) Dash, W.C., J. Appl. Phys. 30, 459 (1959).

86) Scace, R.I., and G.A. Slack, J. Chem. Phys. 30, 1551 (1959).

87) Newman, R.C. Proc. Phys. Soc. London 76, 993 (1960).

88) Newman, R.C., J. Wakefield, in Metallurgy of Semiconductor Materials (interscience: New York) Ed. J.B. Schroeder 15, p201-8 (1962): J. Phys. Chem. Solids 19, 230 (1961).

89) Baker, J.A., T.N. Tucker, N.E. Moyer, and R.C. Buschert, J. Appl. Phys.39, 4365 (1968).

90) Bond, W.L., and W. Kaiser, J. Phys. Chem. Solids 16, 44, (1960).

91) Newman, R.C., and J.B. Wills, J. Phys. Chem. Solids, 26, 373 (1965).

92) Newman, R.C., and R.S. Smith, J. Phys. Chem. Solids, 30, 1493 (1969).

93) Dawber, P.G., and R.J. Eillott, Proc. Roy. Soc. A273, 222 (1963): Proc. Phys. Soc. London 81, 453 (1963).

94) Newman, R.C., Infrared studies of crystal defects (London, Taylor and Francis) p1-187 (1973).

95) Newman, R.C., and R.S. Smith, J. Phys. Chem. Solids, 30, 1493 (1969).

96) Newman, R.C., and R.S. Smith, J. Phys. Chem. Solids, 30, 1493 (1969).

97) Bean, A.R., and R.C. Newman, J. Phys. Chem. Solids 32, 1211 (1971).

98) Bullough, R., and R.C. Newman, Rep. Prog. Phys. 33, 101 (1970).

99) Newman, R.C. Proc. Phys. Soc. London 76, 993 (1960).

100) Bean, A.R., and R.C. Newman, J. Phys. Chem. Solids 32, 1211 (1971).

101) Bean, A.R., and R.C. Newman, J. Phys. Chem. Solids 33, 1211 (1971).

102) Heimreich, D., and E. Sirtl, Semiconductor Silicon 1977, Proc. 3rd Int. Sym. on Silicon Mat. Sci. and Tech. Ed. H.R. Huff and E. Sirtl, (New York: Electrochem. Soc.) p626 (1977).

103) Bean, A.R., and R.C. Newman, J. Phys. Chem. Solids 33, 1211 (1971).

104) Newman, R.C., A.S. Oates and F.M. Livingston, J. Phys. Latt. 18, L667 (1983).

105) Newman, R.C., J. Phys. C: Solid State Phys. 30, L967, (1985).

106) Fubs, U. Holzhauer, S. Mantl, F.W. Richter, and R. Sturm, Phys. Stat. Sol. (b) **89,** 69(1978).

107) Dannefaer, S., and D. Kerr, Oxygen in Silicon: A positron annihilation investigation. J. Appl. Physics 60 (4) (1986).

108) Kaiser, W., H.L. Frisch, and H. Reiss, Phys. Rev. **112,**1546 (1958).

109) Oehrlien, G.S., and J.W. Corbett, Mat. Res. Soc. Symp. Proc. 14, 107, Eds. S. Mahajan and J.W. Corbett, (Elsevier Sciene Publ., New York, 1983).

110) Ourmazd, A., and M. Kanamari, J. Appl. Phys,. 56, 1670 (1984).

111) Kanamri, A., and M. Kanamri, J. Appl. Phys., 50, 8095 (1979).

112) Oehrlien, G.S., and J.W. Corbett, Mat. Res. Soc. Symp. Proc. 14, 107, Eds. S. Mahajan and J.W. Corbett, (Elsevier Sciene Publ., New York, 1983).

113) Ourmazd, A., and M. Kanamari, J. Appl. Phys,. 56, 1670 (1984).

114) Wezep, D., J. Csregorkiewiez, H. Be Kman, and C. Ammeriaan, Proc. Inter. Conf. on Defects in Semiconductors, Paris, 1986, Ed. by H.J. Van Bardeleben, in: Mater. Sci. Forum , 10-12, 1009 (1986).

115) Kimerling, L.C., in: Oxygen, Carbon, Hydrogen and Nitrogen in Crystalline Silicon (Proc. Conf., Boston, MA (1985), pulb. by MRS, Pittsburgh, PA (1986), p83 (Symp. Proc. Series, vol. 59).

116) Svensson, J., B.G. Svensson, and J.L. Lindstrom. Appl. Phys. Lett. 49, 1435 (1986).

117) Lindstrom, J.L., G.S. Oehrlein, and J.W. Corbett, Phys. Ststatus Solidi A95 179(1986).

118) Lindstrom, J.L., and B.G. Svensson, in: Oxygen, Carbon, Hydrogen and Nitrogen in Crystalline Silicon (Proc. Conf., Boston, MA (1985), pulb. by MRS, Pittsburgh, PA (1986), p45 (Symp. Proc. Series, vol. 59).

119) Deleo, G.G., C.S. Milsted Jr, and J.C. Kralik, Phys. Rev. B31,1588 (1985).

120) Dannefaer, S., G.W. Dean, D.P. Kerr, and B.G. Hogg, Phys. Rev. B14, 2709 (1976).

121) Dannefaer, S., S. Kupca, B.G. Hogg, and D. Keer: Phys. Rev. 22, 6135 (1980).

122) Dannefaer, S.: J. Phys. C15, 599 (1982).

123) Dannefaer, S., N. Fruensgaard, S. Kupca, B.G. Hogg, and D. Kerr:Can. J. Phys., 61, 451 (1983).

124) Dannefaer, S., and D. Kerr: Mat. Science Forum, 10-12, 103 (1986).

125) Mascher. P., S. Dannefaer, and D. Kerr: Mat. Science Forum, 38-41, 1157 (1989).

126) Dannefaer, S., and D. Kerr: J. Appl. Phys., 60, 1313 (1986).

127) Dannefaer, S.:Phys. Stat. Sol. 102, 481 (1987).

128) Dannefaer, S.: Proc. Int. Conf. the Science and Technology of Defects Control in Semiconductors (Elsevier Science Publ. B.V. , Amusterdam, 1990) p 1561.

129) Corbett, J.W., P. Deak, J.L. Lindstrom, L.M. Roth, and L.C. Snyder in: Defects in Semiconductors Ed. by G. Ferenezi, Material Sci. Forum, 38-41, 579 (1989).

130) Dannefaer, S., and D. Kerr, J. Appl. Phys. 60, 1313 (1986).

131) Dannefaer, S., W. Puff, P. Mascher, and D. Kerr, J. Appl. Phys. 66, 3526 (1989).

132) Dannefaer, S., and D. Kerr, J. Appl. Phys. 60, 1313 (1986).

133) Dannefaer, S., in: Defects Control in Semiconductors, Ed. K. Sumino (Elsevier Science Publ. Amsterdam, 1990) p.1561.

134) Mascher, P., S. Dannefaer, and D. Kerr, Phys. Rev. B40, 11764 (1989).

135) Dannefaer, S., and D. Kerr, J. Appl. Phys. 60, 1313 (1986).

136) Dannefaer, S., in: Defects Control in Semiconductors, Ed. K. Sumino (Elsevier Science Publ. Amsterdam, 1990) p.1561.

137) Patel, J.R., in: Semiconductor Silicon, Eds. H.R. Huff and E. Sirtl (Electrochem Soc.,

Princeton, 1977), p.521.

138) Newman, R.C., MRS Symp. Proc. 1986, vol. 59, p.403.

139) Claeys, C., and J. Vanhellemont, Solid State Phenomena, 667, 21 (1989).

140) Shimura, F., J.P. Baiarda, and F. Fraundorf, Appl. Phys. Lett. 46, 941 (1985).

141) Urli, N.B., and B. Pivac, Rad. Effect and Defects in Solids 111,112, 449 (1989).

142) Dannefaer, S., and D. Kerr, Oxygen in Silicon: A positron annihilation investigation. J. Appl. Physics 60 (4) (1986).

143) Dannefaer, S., in: Defects Control in Semiconductors, Ed. K. Sumino (Elsevier Science Publ. Amsterdam, 1990) p.1561.

144) Gosele, U., and T.Y. Tam in: Defects in Semiconductor II, Eds. S. Mahajan and J.W. Corbett, (Elsevier Science Publ. Amesterdam 1983) p.153.

145) Nichols, C.S., C.G. Van de Walle, and S. T. Pantelides, Phys. Rev. Lett. **62,** 1049 (1989).

146) Dannefaer, S., P. Mascher, and D. Kerr, Phys. Rev. Lett., **56,** 2195 (1986).

147) Dannefaer, S., D. Kerr, and B.G. Hogg, J. Appl. Phys., **54,** 155 (1983).

148) Makinen, J., C. Corbett, P. Hautojarvi, P. Moser, and F. Fierre, Phys. Rev. B (1989).

149) Peterson, K., "Crystal Defects Studied by Positrons" Ph.D. Thesis (1978) Lab. of Applied Physics II, Technical University of Denmark, DK-2800 Lyngby, Denmark. p.14,19.

150) Dannefaer, S.,"Positron Annihilation in Coloured and Uncoloured KCl and NaCl", Ph.D. Thesis (1972) Lab. of Applied Physics II, Technical University of Denmark, DK-2800 Lyngby, Denmark. p.10,34.

151) Corbett, J.W., and J.C. Bourgoin, in: Defect Creation in Semiconductors, Eds. J. Crawford, Jr., and L.M. Slifkin, vol. 2 (Publ. Plenum Press, New York 1975) p.27,30.

152) Mikkelsen, J.C. JR., MRS Symp. Proc. 1986, vol. 59, p.3.